SFH80 A103038 –Open

REPORT

Field demonstration of a novel towed, area bubble-plume zooplankton (*Calanus sp.*) harvesting approach

Eduardo Grimaldo[a]*, Ira Leifer[b], Svein Helge Gjøsund[a], Roger B Larsen[c],Henrik Jeuthe[c]

SINTEF Fisheries and Aquaculture
Fisheries Technology

May 2010

SFH80 A103038

REPORT

Field demonstration of a novel towed, area bubble-plume zooplankton (*Calanus sp.*) harvesting approach

Eduardo Grimaldo[a*], Ira Leifer[b], Svein Helge Gjøsund[a], Roger B. Larsen[c], Henrik Jeuthe[c]

SINTEF Fisheries and Aquaculture
Fisheries Technology

May 2010

SINTEF

SINTEF

SINTEF Fisheries Technology
Fish Technology

Address: NO-7465 Trondheim, Norway
Location:
SINTEF Sealab
Brattørkaia 17C

Telephone: +47 4000 5350
Fax: +47 932 70 701

E-mail: fish@sintef.no
Internet: www.sintef.no

Enterprise No.: NO 980 478 270 MVA

SINTEF REPORT

TITLE

Field demonstration of a novel towed, area bubble-plume zooplankton (*Calanus sp.)* harvesting approach

AUTHOR(S)

Eduardo Grimaldo [a]*, Ira Leifer[b], Svein Helge Gjøsund[a], Roger B. Larsen[c], Henrik Jeuthe[c]

CLIENT(S)

The Research Council of Norway

REPORT NO.	CLASSIFICATION	CLIENTS REF.	
SFH80 A103038	Open	Nina Hedlund	
CLASS. THIS PAGE	ISBN	PROJECT NO.	NO. OF PAGES/APPENDICES
Open	978-82-14-04949-7	830179	37
ELECTRONIC FILE CODE		PROJECT MANAGER (NAME, SIGN.)	CHECKED BY (NAME, SIGN.)
Document2		Svein Helge Gjøsund S.H.G.	Thomas McClimans Thomas McClimans
FILE CODE	DATE	APPROVED BY (NAME, POSITION, SIGN.)	
	2010-05-25	Vegar Johansen, Research Director Vegar Johansen	

ABSTRACT

This paper presents field experiment results of using a new technology to harvest copepods (*Calanus sp.)* in the ocean by bubble upwelling. Two large-scale bubble rafts, a 21 m^2 and a flexible 75 m^2 bubble raft with tow parallel and perpendicular sparger elements, respectively, were field tested in areas with high, upper 25-m water column *Calanus* densities. Measured bubble-driven upwelling velocities (V_{up}) at different air flows (Q) and depths (z_0), found $V_{up} \sim Q^{0.27}$ under stratified marine conditions, in agreement with other results for stratified conditions. Bubble trawls significantly enhanced *Calanus* concentrations in the upper water column, as much as 1416% integrated over the upper 2-m, with the best results for the tow-transverse raft, which also was tested under unstratified seas. Bubble trawl performance also was related to stratification with the highest enhancement for the lowest stratification. Catch species analysis showed reduced bycatch. Thus, this new harvesting technology showed a potential to develop an economically robust, environmentally benign, and sustainable fishery on a renewable resource at lower trophic levels in the food web, within the context of ecosystem-based management.

KEYWORDS	ENGLISH	NORWEGIAN
GROUP 1	Harvesting Zooplankton	
GROUP 2	*Calanus*	*Calanus*
	Air bubbler	Luftbobbler
	Bubble plume	Plume
	Upwelling Velocity	Upwellingshastighet

TABLE OF CONTENTS

Field demonstration of a novel towed, area bubble-plume zooplankton (*Calanus sp.)* harvesting approach

Eduardo Grimaldo [a]*, Ira Leifer[b], Svein Helge Gjøsund[a], Roger B. Larsen[c], Henrik Jeuthe[c]

[a] SINTEF Fisheries and Aquaculture, NO-7465 Trondheim, Norway.
[b] Marine Sciences Institute, University of California, Santa Barbara, CA, 93106, US
[c] University of Tromsø, Breivika NO-9037 Tromsø, Norway
* Tel: +47 40624014, E-mail: Eduardo.Grimaldo@sintef.no

ABSTRACT

This paper presents field experiment results of using a new technology to harvest copepods (*Calanus sp.)* in the ocean by bubble upwelling. Two large-scale bubble rafts, a 21 m^2 and a flexible 75 m^2 bubble raft with tow parallel and perpendicular sparger elements, respectively, were field tested in areas with high, upper 25-m water column *Calanus* densities. Measured bubble-driven upwelling velocities (V_{up}) at different air flows (Q) and depths (z_0), found $V_{up} \sim Q^{0.27}$ under stratified marine conditions, in agreement with other results for stratified conditions. Bubble trawls significantly enhanced *Calanus* concentrations in the upper water column, as much as 1416% integrated over the upper 2-m, with the best results for the tow-transverse raft, which also was tested under unstratified seas. Bubble trawl performance also was related to stratification with the highest enhancement for the lowest stratification. Catch species analysis showed reduced bycatch. Thus, this new harvesting technology showed a potential to develop an economically robust, environmentally benign, and sustainable fishery on a renewable resource at lower trophic levels in the food web, within the context of ecosystem-based management.

Key words: Harvesting Zooplankton; *Calanus*; Air bubbles; Bubble Plume; Engineered Upwelling; Upwelling Velocity.

1 Introduction

1.1 Overview

In recent years there has been increased interest in the exploitation of marine zooplankton like copepods and krill. This has been motivated by the increasing demand for marine bio-resources for human consumption in general, and in particular the growing demand for feed in aquaculture. In Nordic Seas, zooplankton are a key component in the energy transfer from primary producers to higher trophic levels such as herring, capelin, salmon, cod larvae and juveniles, and other species (Skjoldal, 2005). Roughly 70-80% of the zooplankton production in these waters is made up by copepods of the genus *Calanus* (Tande and Miller, 2000). According to general ecological theory about 10% of this production is available to the next trophic level (Lalli and Parsons, 1997). Estimates of the total annual production of *Calanus* sp. vary between 75 million tons y^{-1} for the Nordic Seas (Aksnes and Blindheim 1996) and 300 million tons *Calanus* spp. (mainly *C. finmarchicus*) y^{-1} for the Norwegian Sea only (Skjoldal et al. 2004). This vast resource has great economic potential because it is rich in marine lipids, proteins, amino acids, and pigments. Further, by nature of being low on the food chain it has far lower bioaccumulation of heavy metals, organo-chlorides, dioxins, and other pollutants than higher trophic species now in use (Mizukawaa et al., 2009). Therefore, copepod fisheries have a potential to support the growth of new ventures in markets for functional food, food ingredients, and nutrition products. However, development of a copepod fishery must be pursued wisely (Nicol and Endo, 1999) using the best technology at hand, and implemented within a solid ecosystem based management regime, particularly given the importance of copepods to the marine ecosystem.

In open Norwegian waters, *Calanus spp.* are widely found in the upper 50 m during the productive period from April to August (Falkenhaug et al., 1997; Dahle and Kaartvedt, 2000). For practical reasons, harvesting concentrates on adults (CVI) and the life stages CIV and CV (the two last copepodite stages before becoming adults), because in these stages copepods have achieved sufficient body mass - body lengths are from 2.3 to 5.0 mm, depending upon species (Unstad and Tande, 1991). In addition, lipid content of copepods increases with increasing stage, with the two oldest stages being the most lipid rich (Kattner and Krause 1987).

Currently, *Calanus* harvesting uses fine-meshed trawls (~500 µm bar length) with mouth openings that range from 40 to 100 m^2, depending on the vessel size (Snorre Angell, Calanus AS, Sortland-Norway, Pers. Comm., 2009). However these trawls may be unsuitable for large-scale zooplankton harvesting because their very high towing resistance translates to high fuel consumption and CO_2 emissions. Moreover, several unwanted species are included in the harvested biomass. This study presents field test results of a new fisheries approach, incorporating bubble flotation in the harvest process to greatly reduce costs and significantly reduce negative ecological impacts.

The goal of bubble flotation-enhanced harvesting is to use bubbles to collect and vertically transport *Calanus* from a range of depths, depositing and concentrating them in a thin surface or mid-depth layer. Vertical concentration increases zooplankton harvesting efficiency by increasing the catch for a given trawl opening and resistance. In addition,

bubbles are far less efficient at collecting and transporting larger species, such as fingerlings, which thus will be concentrated less or not at all in the *Calanus* target layer, i.e., the approach provides species selectivity. Also, bubbles can be used to lift jellyfish out of the trawl path, preventing them from clogging the net.

1.2 Air bubble technology /Bubble-driven upwelling / Engineered bubble plumes

The two primary mechanisms underlying a bubble fishery are upwelling (Leifer et al., 2009) and attachment/flotation. As bubbles rise, they transfer momentum to the surrounding fluid, creating the upwelling flow, which transports deeper water upwards, including entrained zooplankton. For bubble attachment, small bubbles attach and add positive buoyancy to the zooplankton, lifting them upwards. Real-world applications involve both of these synergistic processes.

1.2.1 Attachment flotation

Bubbles effectively accumulate surfactants through the process termed sparging or flotation. Surfactants are surface active substances including surfactant-bacteria and particles with hydrophilic and hydrophobic sites that energetically prefer to be at air-water interfaces. This bubble collection and transport process is central to wastewater treatment microflotation (Persechini et al., 2000), mining airlift separators (Mao and Yoon, 1997), bioreactors (Wu, 1995), and marine aggregate formation (Mari, 1999). Surfactants affect bubble properties, decreasing gas exchange and rise velocity and thus decreasing dissolution (Leifer and Patro, 2002). Surfactants also stabilize bubbles against dissolution (Johnson and Cooke, 1980).

Attachment requires several steps. First, the bubble trajectory must intersect the zooplankton close enough for the two to touch. Then, the bubble and zooplankton must attach, rather than "bounce." Finally, the bubble must remain attached for long enough to lead to significant vertical rise. Smaller bubbles are more likely to attach to *Calanus* because of their slower rise velocities, and because their size is comparable to key *Calanus* dimensions, such as thorax, legs, and antennae. However, because small bubble buoyancy is minimal, they provide little lift force. Given that *Calanus* are slightly negatively buoyant; this can lead to small or negligible upwards motion unless several small bubbles attach to the copepod. Laboratory studies showed that highest zooplankton attachment was attained for bubbles with equivalent spherical radius, r, was $50 < r < 300$ µm (own data, unpublished). Larger bubbles have greater buoyancy, however, lower attachment probability (own data, unpublished). Bubbles comparable in size or larger than *Calanus* - circa 1000-µm radius - have well developed turbulent wakes and boundary layers and rise fast, 25 – 30 cm s^{-1} (Leifer and Patro, 2002). These bubbles tend to displace the *Calanus* along streamlines around the bubble as they pass, leading to negligible attachment probability.

After attachment, the bubble-copepod aggregate rises with a velocity, V_{AG}, determined by the drag resistance of the *Calanus*-bubble aggregate and the buoyancy force, until bubble detachment (or surfacing). In laboratory studies, a linear relationship was found between r and V_{AG}, from 2.5 to 9.0 cm s^{-1} with the highest rise velocity for a 341-µm radius bubble (own data, unpublished). Because *Calanus* are mobile, bubble detachment can be significant, occurs by body motions, and reduces the *Calanus* vertical advection distance.

Then, *Calanus*'s negative buoyancy and likely active swimming towards its original depth will cause *Calanus* to descend. Thus, for successful flotation, the attachment time needs to be sufficiently shorter than the detachment time. Due to detachment, more active *Calanus* are lifted less efficiently, mimicking natural selection.

1.2.2 Upwelling Flotation

For sufficiently high bubble concentration, synergistic interactions produce bubble plumes with distinct properties from the surrounding fluid (Leifer et al., 2006). Bubble plumes transfer momentum to the surrounding fluid; creating an upwelling flow, see review in Leifer et al. (2009). The upwelling flow decreases bubble gas exchange with the surrounding fluid because of the reduced transit time across the water column, leading to bubbles surviving longer against dissolution (Leifer et al., 2006). For point-source bubble plumes, fluid velocities are at a peak along the centerline and decrease radially with a Gaussian profile (Milgram, 1983). The fluid velocity increases with height above the source in non-stratified fluids due in part to the increase in buoyancy flux from decreasing hydrostatic pressure. At the surface, the upwelled fluid spreads out in a horizontal intrusion, the outwelling flow.

Thermal and haline stratification are common in the marine environment, with cooler and/or more saline (denser) water at greater depth. Thus, marine upwelling flows lift water with increasingly negative buoyancy. Upon encountering a steep density gradient, the bubble plume can significantly (or completely) detrain plume fluid into a horizontal intrusion; however, the bubbles continue rising, entraining new water, unlike for a continuum (single phase) plume such as a sewage outfall (McDougall, 1978). Such horizontal intrusions deposit any transported zooplankton, marine particles, and dissolved gases in a layer, and have been identified in the field (Solomon et al., 2009; Leifer and Judd, 2002; Leifer et al., 2009). Sufficiently strong bubble plumes can support the upwelling fluid through the density stratification to the sea surface.

Most published bubble plume studies are for stationary bubble plumes in static water (e.g., lake destratification studies) (Schadlow, 1992; Lemckert and Imberger, 1993; Singleton et al., 2007), natural marine hydrocarbon seeps (Leifer et al., 2000a; Leifer and Boles, 2005; Leifer et al., 2009), or gas blowouts (Topham, 1975; Milgram, 1983). However, typical fisheries applications involve a towed bubble plume. There is a significant difference between a stationary plume in a current and a towed plume in stationary water, even though both geometries appear similar (Fig. 1). For the former, each bubble rises and is advected by the currents. As a result, the fluid motions and bubble plume motions are aligned along the plume axis. This allows the bubbles to accelerate the fluid throughout the entire water column. In contrast, for quiescent water, bubbles rise vertically. Thus, for a towed source, the rise angle is vertical as are the fluid motions; however, they are not aligned with the angle of the plume. As a result, a parcel of water experiences vertical advection as a short pulse from the passing bubble sheet, rather than a sustained force. Thus, a towed bubble plume is more analogous to a bubble plume pulse in a current, locally the two are identical; however, the boundary conditions are different. For a stationary bubble plume in a current, the bubble plume is surrounded by water with no vertical motion. In contrast, in a towed plume the "local" bubble pulse is bounded on the down-tow side by persistent upwelling

flows driven by the pulse that already passed. As a result, momentum exchange between the bubble plume and ambient fluid largely occurs only on the up-tow side. Where the upwelled fluid forms a mid-water column or surface horizontal intrusion, this interaction leads to different flow patterns than associated with a stationary bubble plume in a current.

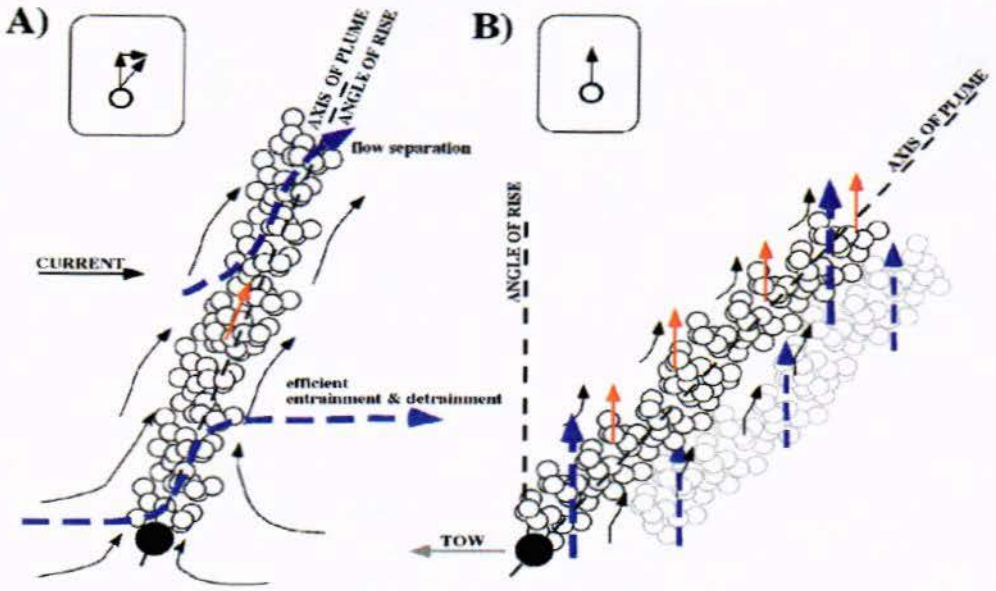

Fig. 1 Schematic showing bubble plume for **A)** fixed point source and **B)** towed source. Inset shows details of individual bubble motions. Red and black arrows pertain to bubbles and entrained water, respectively. Grayed bubbles represent plume several seconds earlier, and remnant, persistent fluid motions.

2 Materials and Methods

2.1 Location

Two field tests were conducted from the *R/V Jan Mayen*, a 63.8-m, 4080-HP stern trawler to better understand the fluid dynamics associated with towed area bubble plumes. Towing tests were off the coast of Nordland (Andfjord) in northern Norway, 16–25 June 2008 (69°07.470'N, 16°00.836'E) with assistance by an auxiliary zodiac, and 22 April – 05 May 2009, (69°08.006' N, 16°07.856 E) by the *R/V Hyas* (12.24 m 250 HP) (Fig.2)

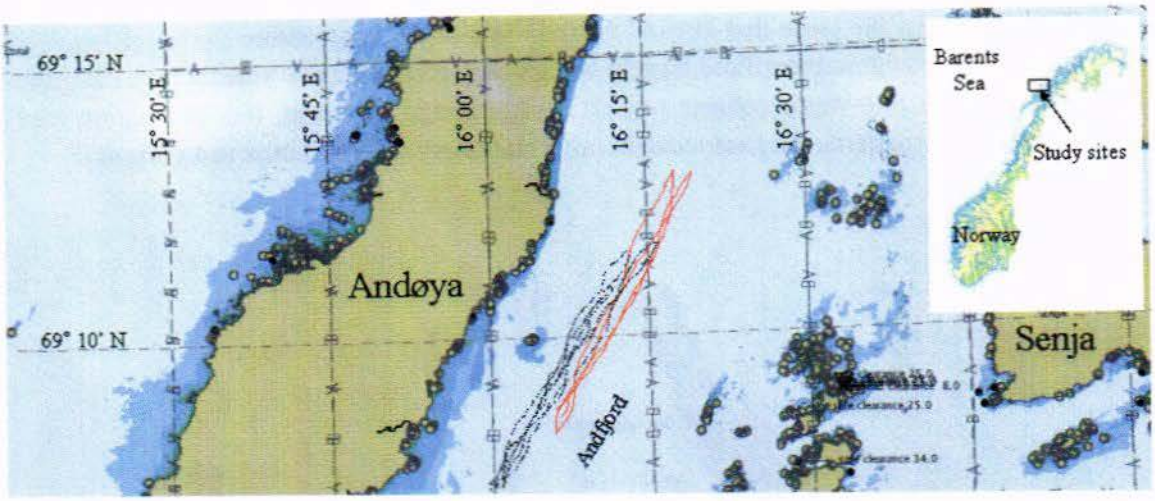

Fig. 2. Map showing location of study area. The dotted line shows the trajectory followed by the *R/V Jan Mayen*. Dotted black and solid red lines for 2008, and 2009 experiments, respectively.

Wind, wave, and meteorological conditions were recorded periodically every few hours, or when significant changes occurred. Weather conditions were highly favourable for the upwelling experiments on 20 June 2008; winds were calm and seas were flat. For the 25-m tow-tests on 22 June 2008, winds were up to 4 m s^{-1} and swell was ~0.5 m, primarily in the afternoon, while the following day for the 15 and 10-m tow tests winds reached ~6 m s^{-1} in the afternoon and swell was ~1.25 m. Seagoing conditions were ideal throughout the 2009 cruise, with very low, upper-water turbidity, near calm winds (~2 m s^{-1}), and minimal swell generally <20 cm.

2.2 Towed bubble rafts

Key system components are a submerged, towed air bubbler area diffuser, termed *bubble raft*, an air delivery system, and a collector net or surface skimmer. Two bubble raft orientations were deployed, one with the sparger elements parallel to the tow direction, termed *tow parallel bubble raft*, and one with the sparger elements perpendicular or transverse to the tow direction, termed *tow-transverse bubble raft*. A second difference was the size distribution produced, with the tow-parallel bubble raft producing far smaller bubbles than the tow-transverse bubble raft. Both were designed for tow depths from 10 to 30 m at tow speeds of 0.5 to 1.2 m s^{-1}.

2.2.1 Raft with tow-parallel sparging elements

A 21-m^2 bubble raft was constructed to produce very small air bubbles in a large area plume for marine application. Air was introduced into a stream of sea water using a porous cylindrical sparging element placed inside a 50-mm diameter, 0.8-m long stainless steel pipe, which produced a large number of bubbles ~1-2 mm diameter and was mixed with a seawater flow inside the pipe (Fig 3A). The sparging element was an in-tank and/or Intrusive Sparger Element, 24-mm outer diameter, 610-mm long, and Media Grate 2 (Mott

Corporation, USA). Eight bubble sparger/mixers were fixed in parallel with 50-cm separation and attached to a 24-mm (1/2-inch) inner diameter, 6-m rubber hose with a large number of 6-mm holes drilled into it. Three holes were drilled every 10 cm along the hose at approximately equi-angular spacing. Two 3.5-m long aluminium tubes were affixed perpendicular to the sparging elements at the 6-m long raft's front and stern to provide rigidity.

The entire bubble raft was stretched and stabilized during towing by two 0.75 m^2 kites attached to the raft stern (Fig. 3B). Also, four 60-cm buoys were connected by 6-mm polyethylene ropes to the raft corners and helped maintain the bubble raft at the desired towing depth and provided visual location markers.
Air was supplied to the bubble raft through eight 12-mm (1/2-inch) inner diameter, 60-m air lines from a regulator manifold on the towing vessel. The manifold controlled each individual line through eight filter pressure regulators (NORGREN, Olympian Plus B64G) and included flowmeters (FL-2095, Omega Engineering, CT) to monitor the airflow. The flow rate and pressure were recorded for each line before and after each experiment, and generally were stable to better than the flowmeter precision. High pressure air supply to the regulator manifold was from a portable compressor (Mobilair M64, Kaeser, Inc., Germany) with an air delivery capacity of 6.4 m^3 dried air at 7-bar pressure and a regulated temperature of 7°C. Airflows to the raft were up to ~7200 L min^{-1} at STP.

Sea water was supplied from the towing vessel's sea water pump system to the bubble sparger elements by a mainline, 10-mm (4-inch) inner diameter, 60-m rubber hose, which split into eight 24-mm (1-inch) inner diameter, 5-m rubber hoses (Fig. 3B). The seawater flow rate and pressure were controlled on board and recorded before and after each test. Two water flows were tested initially, 1000 and 1400 L min^{-1}; with the latter providing better distribution of the bubble-water mixture over the entire bubble raft. Thus, a water flow of 1400 L min^{-1} was used.

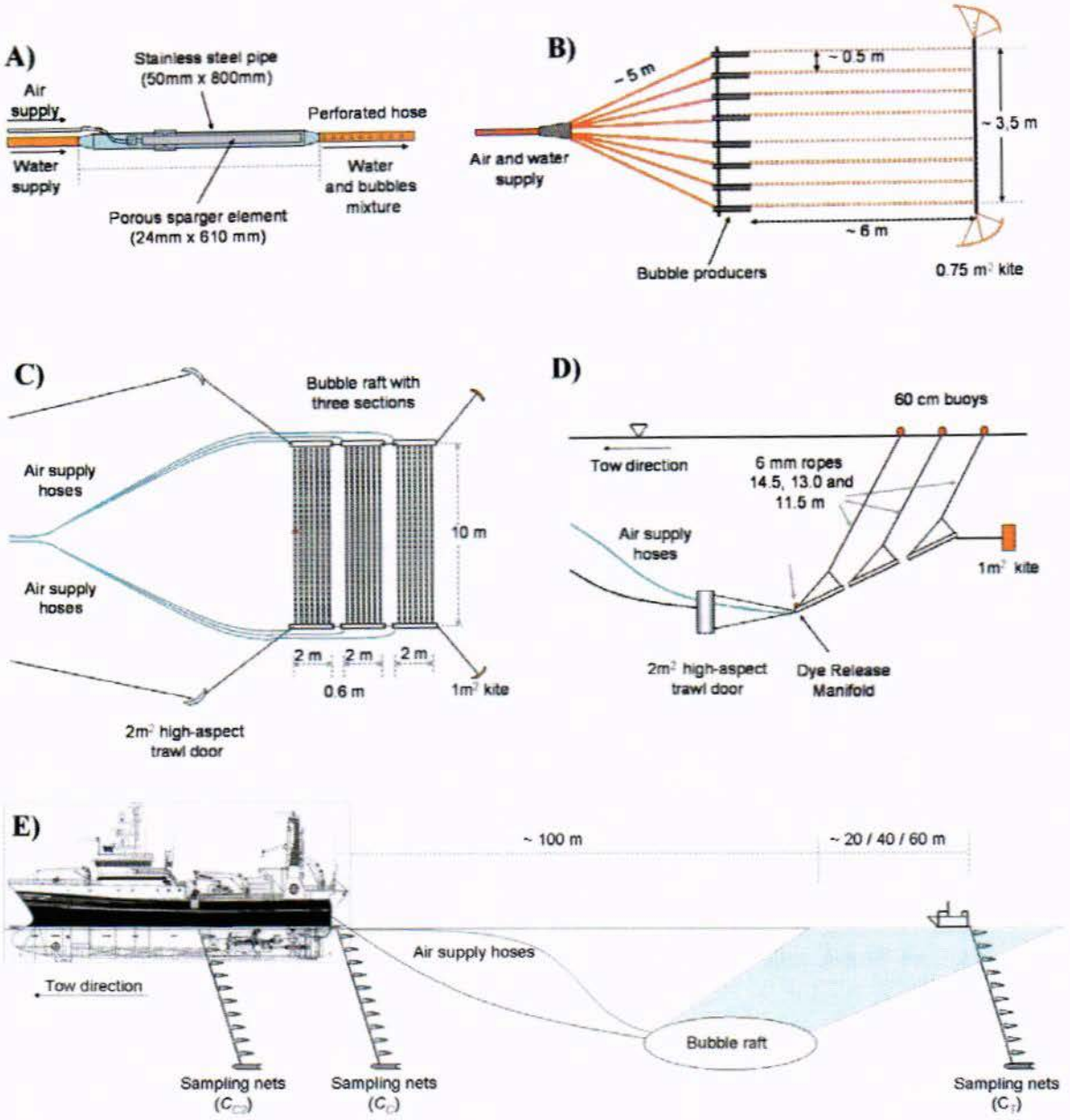

Fig. 3 Schematics for the parallel sparger bubble raft. **A)** Single bubble sparger element. **B)** Top view of the parallel-sparger bubble raft. **C)** Top view of transverse-sparger bubble raft comprised of 3 sub-raft elements and **D)** side view. **E)** Bubble raft and plankton net deployment.

2.2.2 Raft with tow-transverse sparging elements

A second, 75 m^2 bubble raft was designed to generate a more homogeneous area bubble plume of larger bubbles and used transverse sparger elements (Fig. 3C). Bubble sparger elements were porous rubber soaker hoses, 12-mm inner diameter, which were assembled into three identical 25 m^2 raft sections, each with seven 10-m long spargers fixed in parallel and 33 cm apart and held in place by thin nylon strings. Spargers were connected on both ends to a 63-mm rigid PVC pipe, to which high pressure air was supplied from the towing vessel by six 60-m long, 19-mm (¾-inch) diameter air supply hose. The PVC pipes provided some structural stiffness as well as distributing the air from the air supply line to both ends of the 7 sparger elements, through two air supply lines for each raft section. The three raft sections were rigged to maintain an ~35° inclination angle while under tow. This angle was chosen to match typical bubble rise velocities in the bubble plume for a tow speed of 0.5 m s^{-1}, thus the raft continuously injects bubbles into the rising bubble sheet. The raft was designed with significant flexibility between sections to facilitate deployment/recovery.

Raft configuration (Fig. 3D) was maintained during towing by two 1 m^2 kites attached to rear corners of the raft, two, 2 m^2 high-aspect-ratio trawl doors attached to the front corners, and a series of 6-mm polyethylene ropes of different lengths attached to 60-cm buoys. Each bubble raft section was separated by 0.6 m. The raft was towed at a constant 15±0.25 m depth, which was monitored with a pressure sensor (Model MP4-D, Scanmar AS, Norway).

The airflow of each supply hose was filtered, controlled, and measured by a regulator manifold similar to that described in section 2.1. Flow rate and pressure were recorded for each line before and after each experiment, and generally were stable to less than measurable. Air was provided as for 2008, and flows up to 8430 L min^{-1} (STP) were produced with this setup.

2.3 Upwelling measurements

Upwelling flow $<V_{up}>$ measurements were made for the parallel-sparger raft in 20 June 2008 off the coast of Andøya, Norway (69° 02.470'N, 16° 06.836'E) in water with depths between 216 and 307 m (Fig. 2) by injecting dye and measuring the transit time, t, for the dye to reach the sea surface. Values of t were determined with a stopwatch based on the first arrival time at the sea surface, when the boil exhibited green colour (Fig. 4B). Values of t were long compared to the uncertainty due to human error in stopwatch timing, and generally showed a high degree of repeatability. Measurements were made for a range of airflows, Q (2100 to 7200 L min^{-1} at STP-standard temperature and pressure), and release depths, z_0 (2.5, 5.0, and 7.5 m). Each combination had between 3 and 20 repetitions, depending on variability (more repetitions for higher variability data sets). For the transverse sparger bubble raft, the upwelling flow was measured for z_0= 15 m and Q= 8432 L min^{-1} (STP); however, dye surfacing was difficult to observe and $<V_{up}>$ was measured only for this combination.

Dye was injected from a manifold mounted at a central location on both rafts. The manifold was supplied with concentrated fluorescein dye solution through a 60-m long, 6-mm inner

diameter hose. Air, water, and dye supply lines were bundled for better handling, to minimize flow disturbances, and to reduce hydrodynamic resistance during towing.

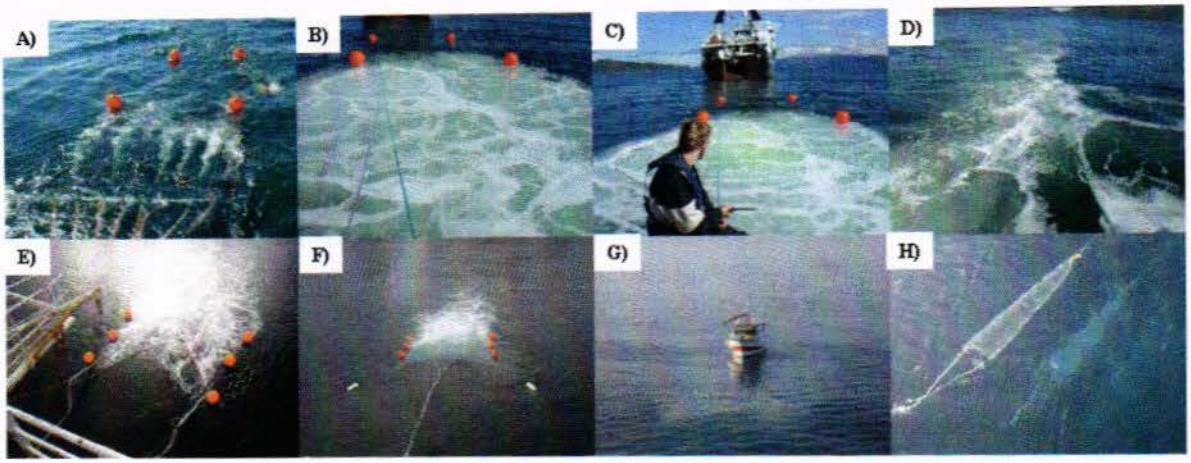

Fig. 4 Photos of parallel-sparger bubble raft **A)** during deployment 20 June 2008, **B)** Surface expression of the bubble plume for 4800 L min^{-1} air from 5-m depth. **C)** Dye arriving at sea surface. Buoys are 60-cm diameter. *R/V Jan Mayen* stern is 120 m distant. **D)** Surface bubble plume for 25 m deployment. Photos of transverse-sparger bubble raft **E)** during deployment on 20 April 2008. **F)** The trawl doors spreading the bubble raft laterally. **F)** *R/V Hyas* in position in bubble plume for sampling. **H)** Tow sampling nets, note high visibility.

2.4 *Calanus* vertical profile measurements

The effect of the bubble-driven upwelling upon the *Calanus* vertical distribution was studied by comparing vertical profiles of *Calanus* catch samples before and after a given area had been trawled with the bubble raft. Standard plankton net (20 cm diameter, 0.5 mm mesh opening) arrays were towed for 30 min periods at sample depths, z_T (Fig. 4H). In 2008, z_T was 0.1, 1.0, 4.0, 7.0, 10.0, 13.0, and 16.0 m; in 2009, z_T was 0.1, 0.5, 2.0, 3.5, 5.0, 6.5, 9.5, 12.5, 15.5, and 18.5 m. For 0.5 m s^{-1} tow speed, a sample net sweeps 28.3 m^3 water. Test samples were collected from the zodiac whose position was maintained by a rope to R/V *Jan Mayen*, 25 m behind the initial upwelling boil and ~125 m behind R/V *Jan Mayen* (Fig. 4B and 4C). The sampling protocol followed involved first deploying the control nets, and then the test nets 60 seconds after the last control net entered the water. Retrieval followed the same order. This allowed the test and control nets to sample approximately the same water. Zodiac collected samples were transported to the *Jan Mayen* for analysis followed by zodiac redeployment. In 2009, samples were collected 20, 40, and 60 m beyond the bubble plume's first surfacing location and analyzed onboard R/V *Hyas* (Fig. 4G). Reference (control) *Calanus* vertical profiles, $C_C(z_T)$, were measured from R/V *Jan Mayen*, while test vertical profiles, $C_T(z_T)$, were measured from the zodiac in 2008 and from R/V *Hyas* in 2009. The biovolume of *Calanus* was analyzed from the sample net catch by first excluding jellyfish, then emptying the sample into 50-ml graduated tubes, decanting water, and finally reading the *Calanus* volume.

In 2009, it was attempted to tow the bubble raft to one side of the *Jan Mayen's* wake to avoid hull flow and propeller wake effects on the vertical *Calanus* distribution. However, these attempts failed due to insufficient warp length available (max 40 m) to achieve the necessary sideways deflection. The *Jan Mayen*'s effect on $C_C(z_T)$ was characterized by comparison with a second control sampling net array, $C_{C2}(z_T)$, deployed on the *Jan Mayen*'s port.

2.5 Bycatch Analysis

In 2008, catch samples were also analysed for bycatch. Samples to 10-ml volume (if available in the nets) were examined under a microscope and species other than *Calanus* were enumerated. Bycatch was divided into the following groups*: Brachyura indet* (true crabs), *Anomura indet* (hermit-, porcelain-, king crabs and squat lobsters), *Euphausiacea indet* (krill), shrimp (mostly juvenile stages), fish larvae and fish egg.

2.6 CTD Vertical Profile

To identify water-column stratification and to monitor water-column changes, profiles of temperature (T), salinity (S), and fluorescence were measured by CTD (SBE 25, Seabird Electronics, Inc.) casts. The CTD was also equipped with a fluorometer (Seapoint Sensors, Inc.)

3 Results

3.1 Bubble plume upwelling velocity

Plume upwelling velocities were measured for the parallel-sparger bubble raft on 20 June 2008 for a range of Q and tow depths, z_o. The measured mean water-column upwelling flow, $\langle V_{up} \rangle$, was ~10 cm s^{-1} for the bubble raft. For the raft, $\langle V_{up} \rangle$ varied as Q^b, with b varying between 0.246 and 0.323 for release depths $2.5<z_o<7.5$ m (Fig. 5). Upwelling flows for $z_o>7.5$ m were unsuccessful at advecting dye to the sea surface, most certainly due to the sharp stratification at 8 m. There was no clear trend in b with respect to release depth. For the entire data set, b was 0.27. Some of the large variability in $\langle V_{up} \rangle$ probably arose from inhomogeneity in the bubble plume by the time it reached the sea surface (Fig. 5). Based on a 0.5 m s^{-1} tow speed for a 6-m raft, the bubble plume can be considered continuous rather than as a pulse if the fluid transit time is less than 12 s. For $\langle V_{up} \rangle$=21 cm s^{-1}, this is true for z_o=2.5 m. For z_o=5 m, the bubble plume but not the fluid will be continuous (bubbles rise ~25 cm s^{-1} faster than the fluid, i.e., ~45 cm s^{-1}). Unfortunately, effects from the pulsed nature of the raft's bubble plume for the deeper depths could not be separated from effects due to complex near-surface stratification.

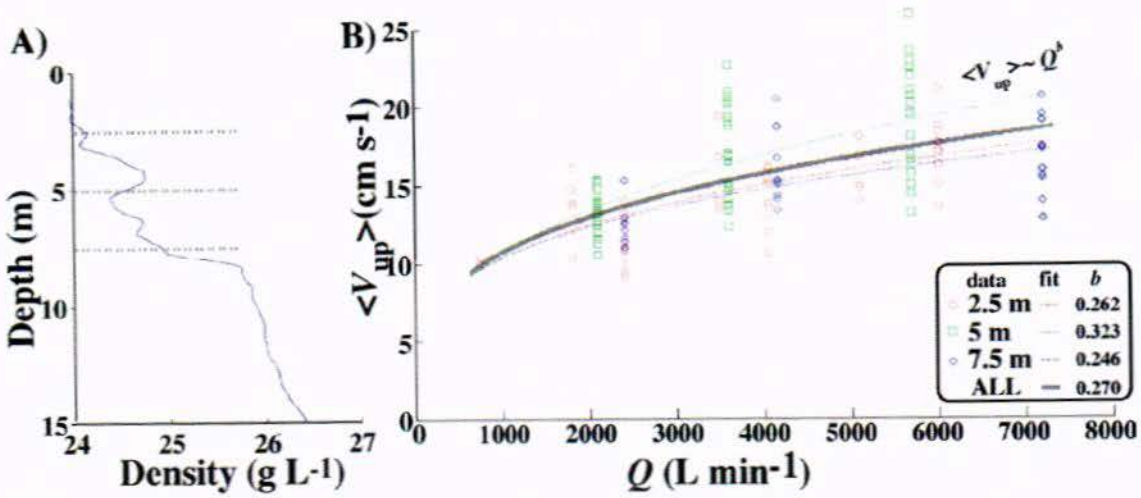

Fig. 5 A) Density depth profile 20 June 2008 (06:36 Local Time). Dashed lines show bubble raft depths. **B)** Upwelling velocity (V_{up}) versus the normalized, total airflow discharge per square meter, Q_A, for the release depths of 2.5, 5, and 7.5 m, and power law fits.

For the transverse-sparger bubble raft, $<V_{up}>$ only was measured for Q=8400 L min^{-1}, the maximum possible flow rate. For z_o=15 m, $<V_{up}>$ was 17.3±2.4 cm s $^{-1}$. Scaling to the smaller area of the parallel-sparger bubble raft, ($Q_{parallel}$=30000 L min^{-1}), predicts $<V_{up}>$~61 cm s^{-1} (neglecting depth differences), i.e., significantly less than implied by scaling from the small raft results. The difference suggests that pulsed bubble plumes are less efficient than continuous bubble plumes, probably because they always are accelerating fluid.

3.2 Bubble-driven upwelling and the vertical *Calanus* distribution

Of the two field studies, the tow-transverse raft performed much better with respect to *Calanus* concentration enhancement. Aiding the tow-transverse raft was negligible stratification in 2009, which also significantly simplified interpretation. In contrast, the 2008 parallel-sparger bubble raft test contended with significant stratification. In addition, the later design performed less efficiently.

3.2.1 Minimally stratified fluid and tow-transverse sparger elements

The initial vertical *Calanus* profiles showed that *Calanus* were distributed primarily in a layer from 4 to 16 m (Fig. 6A, Table 1). After bubble trawling, the bubble plume altered the profile significantly, concentrating *Calanus* in the upper 6 m (Fig. 6B, Table 1). The difference between the control, C_{Cm}, and test, C_T, *Calanus* vertical profiles was highly significant for all three sampling distances (Univariate ANOVA, P<0.001), with total increases of between ~30 and ~130% more *Calanus* for test compared to control sampling nets. The largest *Calanus* concentrations were found for the shallowest test sampling depth (0.1 m).

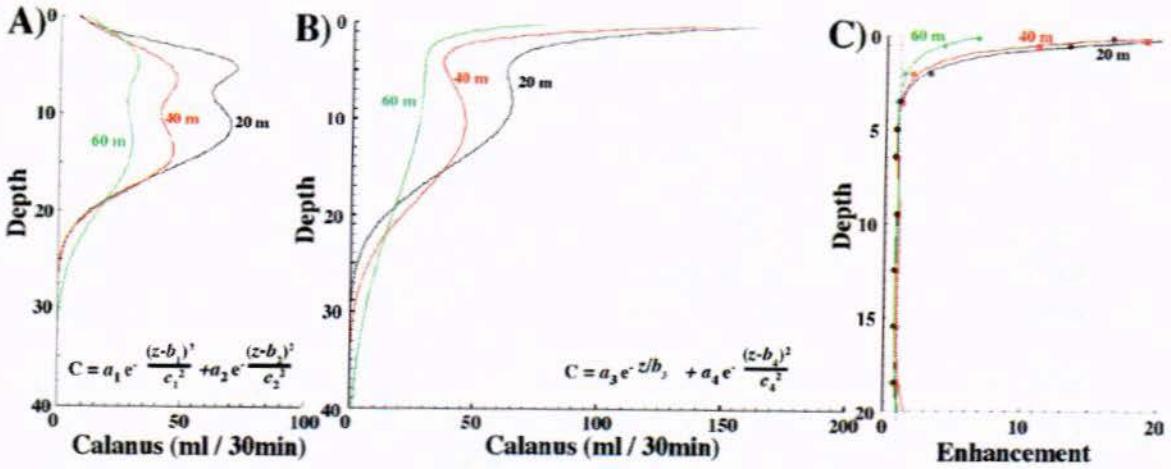

Fig. 6 Curve fits to *Calanus* trawl data for 29-30 April 2009; parameters provided in Table 1. Data is not shown for clarity. **A)** Control plankton nets and **B)** test plankton nets and **C)** Enhancement based on curve fits (line) and data (symbols), at 20, 40, and 60 m behind first bubble surfacing location.

Table 1. Fit parameters for *Calanus* vertical profiles, April 2009

Dist (m)	Time (s)	date	a_1 (ml)	b_1 (m)	c_1 (m)	a_2 (ml)	b_2 (m)	c_2 (m)	R^2 (-)
20*	0	29/04/09	43.12	4.378	2.513	69.65	11.11	6.807	0.959
40*	40	30/04/09	42.13	5.536	4.225	45.54	13.94	5.494	0.972
60*	80	30/04/09	19.64	3.774	3.689	29.71	12.87	9.193	0.972

Dist (m)	Time (s)	date	a_3 (ml)	b_3 (m)	a_4 (ml)	b_4 (m)	c_4 (m)	R^2 (-)
20+	0	29/04/09	135.9	0.5773	63.35	8.524	9.359	0.992
40+	40	30/04/09	129.8	0.8518	45.96	10.37	10.83	0.978
60+	80	30/04/09	49.74	1.088	28.84	5.35	19.71	0.940

* Dual Gaussian fit, eqn(1), + Combined exponential and Gaussian fit, eqn(2).

Along the trawl pathway, background *Calanus*, C_T, were well described by dual Gaussians centered at 4-5 m and 11-13 m with no discernable trend in the layer depths (b_1, b_2) during the field trials; although there was a clear decrease in total water column concentration during the field trials (a_1 and a_2),

$$C_T = a_1 \exp(-((z-b_1)/c_1)^2) + a_2 \exp(-((z-b_2)/c_2)^2) \quad (1)$$

where c_1 and c_2 are the layer half widths. Curve fits are least squares (Matlab curve fit toolbox, Mathworks, MA). This decrease is slightly greater and more consistent for the deeper population (a_2). Interestingly, the double Gaussian layer structure also was found in the chlorophyll (Fig. 7). A curve fit to chlorophyll depth profiles for 29/04/09 found a dual layer with peaks at 8.3 and 16.4 m depth, and layer half widths of 4.79 and 4.69 m,

respectively (R^2=0.95). This shows strong similarity to the *Calanus* data (Table 1) slightly later that day, which showed layers at b_1=4.3 and b_2=11.1 m and half widths of 4.4 and 6.8 m, respectively; thus *Calanus* layers were towards the top of the phytoplankton layers. The phytoplankton clearly was constrained to the upper, well-mixed water column, with density stratification beginning at 18 and 15 m on the two study days, but decreasing to 8 m at the study period end, i.e., just below the bubble raft depth. Thus, although the plume was not working against a significant stratification, some deeper, denser water could have been entrained into the plume during the initial acceleration phase.

There was also a significant spatial increase in the half-width (c_2) of the deeper *Calanus* layer, which spread out, creating a "tail" of individuals extending towards deeper water. At the end of the 2009 study, significant water column change occurred with an increase by a factor of 5 in chlorophyll deeper than 17 m (Fig. 7). This new water may have attracted some of the deeper *Calanus* to extend their range downwards.

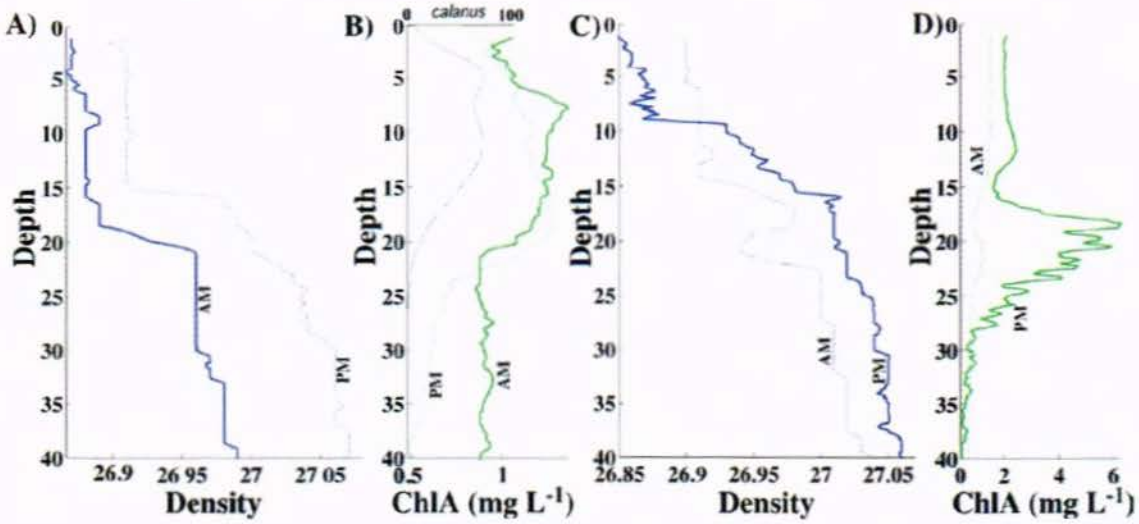

Fig. 7 Vertical profiles on 29 April 2009 (20 m data) of **A)** density and **B)** chlorophyll A and *Calanus* from Fig. 7 for 20 m (black) and on 30 April 2009 (when 40 and 60 m data was collected) of **C)** density and **D)** chlorophyll A.

The effect of the bubble trawl on the *Calanus* was dramatic, particularly at shallower depths, where prior to bubbling there was a near absence of *Calanus*. The data were well fit by a combined exponential and Gaussian, with the transition from exponential to Gaussian at 3-4 m,

$$C_{CM} = a_3 \exp(-z/b_3) + a_4 \exp(-((z-b_4)/c_4)^2) \quad (2)$$

The total number of *Calanus* at the sea surface after the bubble trawl (a_3) decreased with time, in tandem with changes in the control *Calanus* distribution. Also, there was a consistent thickening of the near surface distribution (b_3) with distance (i.e., time) from the plume surfacing location, suggesting that the underlying mechanism causing *Calanus*

enhancement, ε, defined by $\varepsilon=C_T/C_C$, near the sea surface was weakening and broadening and/or allowing *Calanus* to escape and sink. Although the *Calanus* profile decreased during the study, ε accounts for these changes, and was lower for the 60 m than 20 m data. This broadening suggests that fluid motions were controlling the *Calanus* profile because ε had an identical exponential decrease for all three distances. Although the effect of the bubble plumes on the *Calanus* distribution was limited to the upper 3 m (deeper enhancements are ~1.0) there is a significant stretching of the deeper *Calanus* profile (c_4), which is not mirrored in the control profile (c_4). This suggests a bubble-plume related mechanism forcing some *Calanus* downwards.

The enhancement, ε, was highly significant. Specifically, had a 2-m tall *Calanus* net been placed at a depth of 1 m the catch enhancements, $\int_{z=0}^{z=2} \varepsilon \, dz$, would have been 980%, 770%, and 330% compared to a net placed elsewhere in the water column for 20, 40, and 60 m, respectively. Also, the enhancement factor is essentially deeper than the surface layer, suggesting that the much of the *Calanus* enhancement arose from the sides. If the enhancement was from *Calanus* deeper than the surface layer, then the lower concentrations found at deeper depths should have been "advected" to shallower depths, causing a dehancement ($\varepsilon<1$).

3.2.2 Stratified fluid and the parallel-sparger bubble raft

The effect of stratification on a towed bubble plume was investigated during the field studies 22-23 June 2008 in the presence of strong upper water-column stratification (Fig. 8). The stratification also varied during the field study. Similarity in the salinity (Fig. 8C) and density (Fig. 8A) profiles demonstrated salinity control. Temperature varied minimally with time except 22 June 2008, when the water column cooled by ~1°C (largely uniformly with depth and thus not affecting stratification). Stratification changes in the upper 5–7 m showed a tidal variation, saline and well-mixed in the AM, changing to fresher and more uniformly stratified in the PM on both days.

Initially, the water column was well-mixed in the upper 7 m, with slight stratification at ~2-m and an unstably stratified layer, ~1 m thick, at ~8 m depth. Later in the day, though, stratification was more consistent in the upper 15 m. The following morning the vertical density profile returned to a very similar pattern to the previous morning including very sharp stratification at ~8 m, suggesting a tidally driven, evening influx of deeper (high salinity) waters. By afternoon, the upper layer exhibited several step-wise stratifications, through 8 m; with the stratification more uniform to ~20 m depth, below which stratification was weaker.

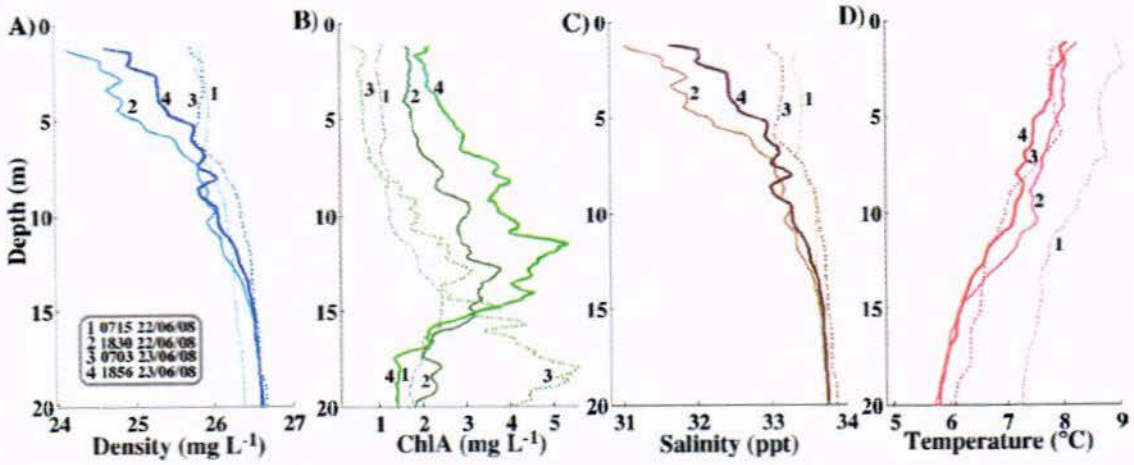

Fig. 8. Depth profiles on 22 June (1 and 2) and 23 June (3 and 4) 2008 for **A)** density, **B)** chlorophyll A, **C)** salinity, and **D)** temperature. Profile times labelled on panel A, dashed lines for morning profiles.

Chlorophyll A concentrations increased towards an asymmetric depth peak that exhibited a tidal trend, varying from 15-m deep at 07:15 LT 22 June to 13 m in the afternoon, then back down to 17 m the following morning (07:02 LT 23 June), becoming shallower again later in the day. In general, the effect of tidal variations in the salinity began at 15 m, thus, tidal water changes likely caused the changes in the chlorophyll A peak.

On 22 June 2008 *Calanus* increased exponentially with depth (C_C=1.26e$^{z/5.7}$, R^2=0.992) with the largest concentrations apparently deeper than 16 m and with few *Calanus* near the sea surface (Fig. 9A, Table 2). This trend roughly paralleled the chlorophyll *A* profile, which increased approximately exponentially until a peak at 16 m in the morning and 13 m in the afternoon. The bubble raft with parallel-sparging elements was towed at 25 m and had a significant effect on the *Calanus* profile, with near sea surface *Calanus* concentrations being only slightly lower than at 16 m. As a result, the exponential increased with z in $C_T(z)$ was far slower with C_T=8.02e$^{(z/41)}$, R^2=0.863. For depths deeper than 14 m, concentrations before and after the bubble raft were similar, while concentrations were higher for shallower depths that corresponded to where the stratification began in the afternoon.

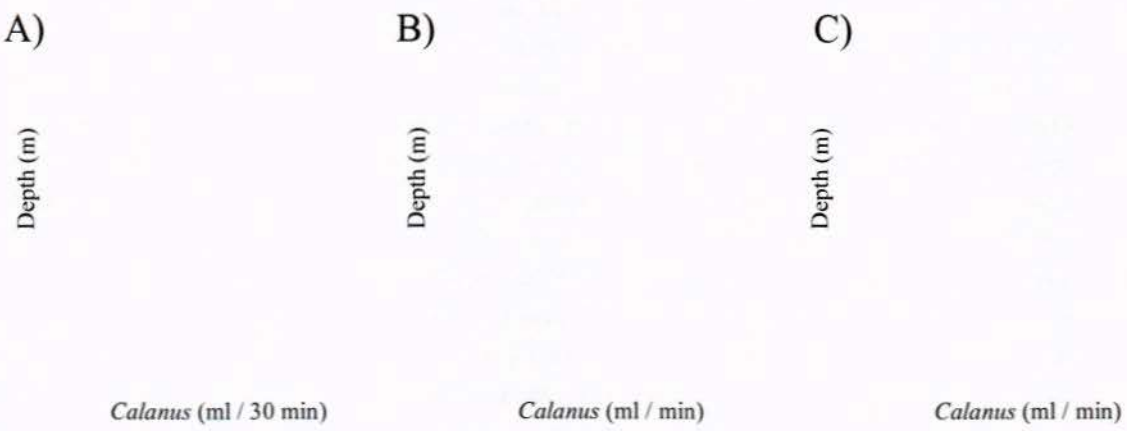

Fig. 9. Mean vertical *Calanus* profile before (C_C, dotted line) and after the bubble trawl (C_T, solid line) for **A)** 25-m tow depth for 22 June 2008. **B)** 15-m and **C)** 10-m tow depth for 23 June 2008. Error bars are 1 standard deviation.

Table 2. Fit parameters for *Calanus* control vertical profiles June 2008.

z_o (m)	Time (s)	a_1 (ml)	b_1 (m)	c_1 (m)	a_2 (ml)	b_2 (m)	c_2 (m)	R^2 (-)
25*	22/06/08	1.258	0.1721					0.989
15+	23/06/08	26.57	5.92	3.497	25.3	20.11	9.381	0.771
10+	23/06/08	23.18	7.795	1.799	11.74	10.71	6.174	0.999

Fit parameters for *Calanus* test vertical profiles June 2008

z_o (m)	Time (s)	a_1 (ml)	b_1 (m)	c_1 (m)	a_2 (ml)	b_2 (m)	c_2 (m)	R^2 (-)
25*	22/06/08	8.021	0.042					0.863
15+	23/06/08	14.50	3.82	4.575	13.98	14.99	5.408	0.916
10*	23/06/08	16.81	7.185	8.75				0.692

* z_o is tow depth. * Exponential Fit. + Dual Gaussian Fit

A more detailed look at C_T shows a dual peak structure in shallow (<5 m) water, with C_T(4 m)>C_T(7 m) (Fig. 9B and 9C). Although the data exhibit significant variability, this depth corresponds to the beginning of the surface stratification layer; water from 3.5 to 7 m was unstratified. These depths correspond to where visual observations from the zodiac sometimes showed the rising green bubble plume billows began drifting rather than continuing to rise. In such case, searching downstream did not reveal their surfacing. For times where bubbles were not surfacing, test nets (zodiac) were positioned to follow the submerged green bubble "shadow." Although sometimes the main plume did not appear to surface, numerous big bubbles (~3-4 mm) always were observed to reach the sea surface, although they did not always produce a boil. Usually, a few seconds later many small bubbles (1-2 mm) surfaced, along with numerous continuous and persistent boils.

On 23 June 2008, the raft was towed at 15 m in the morning, when the upper 6-m of the water column was well mixed, with stratification for depths from 6 to 15 m. The background *Calanus* profile, C_C, was reasonably well-described (R^2=0.77) by a double Gaussian layer, with peaks at 6 and 20 m (extrapolated) and very few *Calanus* in the upper meter (Fig. 9B). The 6-m peak in C_C corresponded to the top of the pycnocline; however, chlorophyll A showed no comparable trend. Although unquantified, there were significant jellyfish in the waters, which could have affected the *Calanus* profile both through avoidance and predation. After the bubble trawl, the profile's double layer character persisted, but was shifted to shallower depths (3.8 and 15 m). Although the upper peak was narrower (4.57 m for C_T versus 5.9 m for C_C); there still were significant *Calanus* in the upper meter. Overall concentrations were lower than before bubbling, particularly between 5 and 9 m (i.e., a layer of stratification), suggesting lateral *Calanus* loss (i.e., plume detrainment) from the bubble plume, or plume entrainment and vertical transport, or both.

The raft was towed at 10 m on the afternoon of 23 June 2008 during which the water-column stratification increased such that after the experiment, stratification was consistent from the sea surface to ~14 m, i.e., deeper than the raft. The background *Calanus* profile, C_C, was described by a thin (3.5 m) strong Gaussian peak at 6 m depth, superimposed over a broader (9.4 m) Gaussian distribution centered at 20.1 m. There was no clear relationship between the 3.5-m layer and water column attributes. After the bubble raft passed, C_T was well described by a single broad (8.8 m) Gaussian centered at 7.2 m, which matched C_C for depths deeper than 10 m (i.e., deeper than the raft). However, if the largest of the three data points acquired for 6 m was an outlier, then C_C and C_T at z_T=6 m would have been comparable. Detailed structure in the density profile showed a sharp stratification at 5 m (and at ~3 m), which correlated with the depths where *Calanus* were enhanced by the bubble raft.

Depth profiles of the enhancement, ε, calculated from the curve fits (Table 2) showed similar trends for the three tow depths (Fig. 10). The 25-m tow, increased as a broad exponential from 15 m to the sea surface, indicating that significant upwelled *Calanus* were detrained from the rising bubble plume throughout the study depths (z<16 m). The shape of the enhancement roughly approximated the shape of the density stratification relative to the tow depth, ρ' (Fig. 10B), at least for the morning profile. Values for $\varepsilon(z)$ for the 15-m tow were decreased (negative) from 12<z<4 m, and showed the lowest surface ε; however, stratification, ρ', also was the smallest of the three tow experiments. The 10-m tow showed the highest surface ε (a_1) and the broadest increase with depth (b_1), i.e., the least concentrated, and lowest values of ε for 6<z_T<10 m. These depths likely correspond to the initial acceleration phase, where *Calanus* are being entrained into the bubble plume making ε<1. The depth where ε exceeded 1 appears roughly related to ρ'; for 10, 15, and 20 m, it was 0.4, 0.6, and 0.3 g L^{-1}, respectively, with the highest value for the profile with the lowest stratification ($d\rho/dz$), i.e., the 15 m tow. Complications with the 25-m tow likely arose from the bubble plume forming boils and the likely significant or complete buoyancy loss due to bubble detrainment and dissolution. Note, uncertainty in interpretation also arises because the density stratification only was measured at the beginning and end of each day's field test.

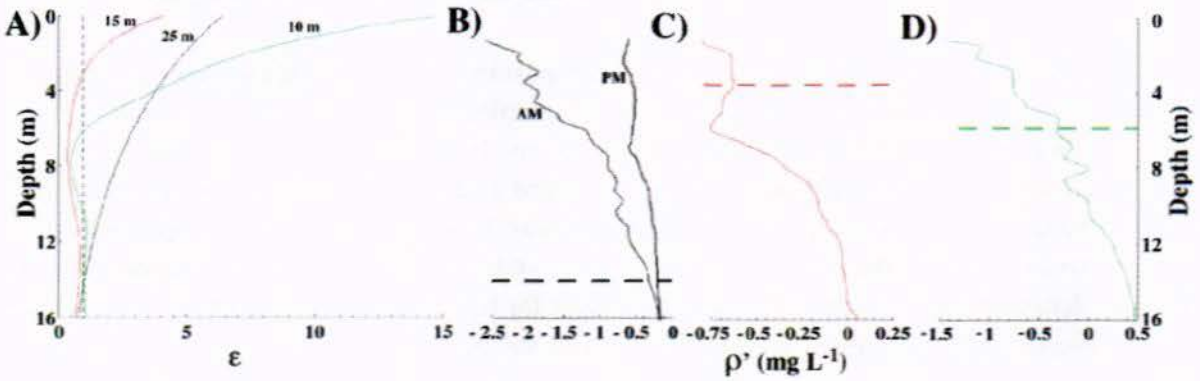

Fig. 10. A) *Calanus* enhancement, ε, depth profiles from data curve fits for 22-23 June 2008. Also shown is the *no enhancement* line (ε=1). **B)** Density difference, ρ', relative to ρ at tow depths of 25 m, **C)** 15 m, and **D)** 10 m. Dashed horizontal lines indicate depth where ε>1.

3.3 Effect of propeller wake on the vertical *Calanus* distribution

The propeller wake's effect on the vertical *Calanus* distribution was assessed on 23 June 2008 and 30 April 2009 by towing the bubble raft **without producing bubbles**. The *Test* plankton nets were towed 20 m behind the behind the bubble plume first surfacing location. No significant difference for the total *Calanus* concentration between C_C, C_{C2}, and C_T was found (Univariate ANOVA, P>0.786); however, shallow *Test* samples caught significantly more *Calanus* than the *Control* nets (Fig. 11), while there was a slight reduction for $4<z<10$ m, suggesting some vertical mixing of the upper water column by the hull.

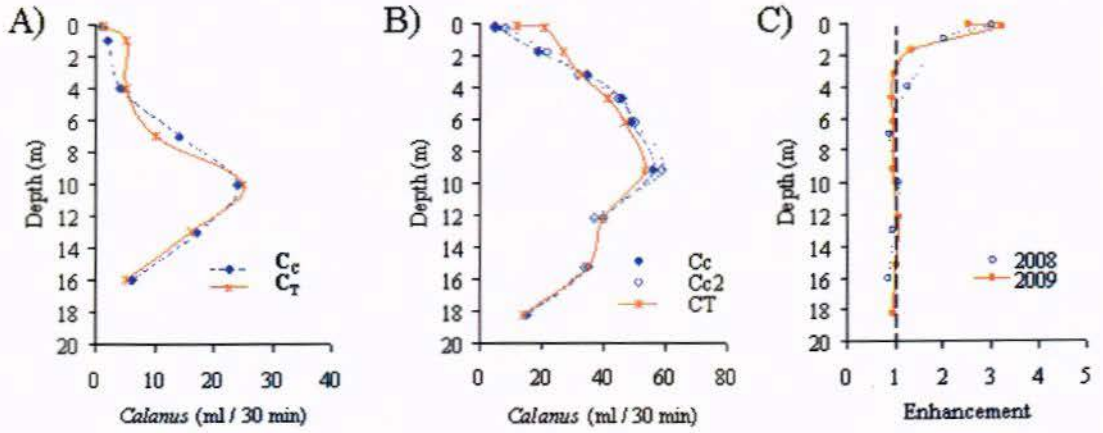

Fig. 11 *Calanus* catches of the *Test* and the *Control* sampling nets, which were collected when towing the bubble raft without producing any bubble plume on **A)** 23 June 2008 and **B)** 30 April 2009. **C)** *Calanus* enhancement, ε, depth profiles from data curve fits for 2008 and 2009. Also shown is the *no enhancement* line (ε=1).

3.4 Effect of bubble-driven upwelling on the vertical distribution of Bycatch

The level of bycatch and its taxonomic composition varied greatly, ranging from none (pure *Calanus*) to ~400 individuals per ml of sample. The most common bycatch was crabs (*Brachyura indet*, *Anomura indet*) at different larval stages. Fish eggs and larvae were present in some samples at levels up to 160 and 8 per ml sample, respectively. However, the value for eggs bears great uncertainty because it was derived from extrapolation of very small sample volumes (0.1 ml). Mean vertical bycatch profile showed significant dehancement ($\varepsilon<1$) for all organisms, except for fish larvae when the raft was towed at 10 m depth. Dehancement rates varied between 48 and 95% (Fig. 12, Table 3).

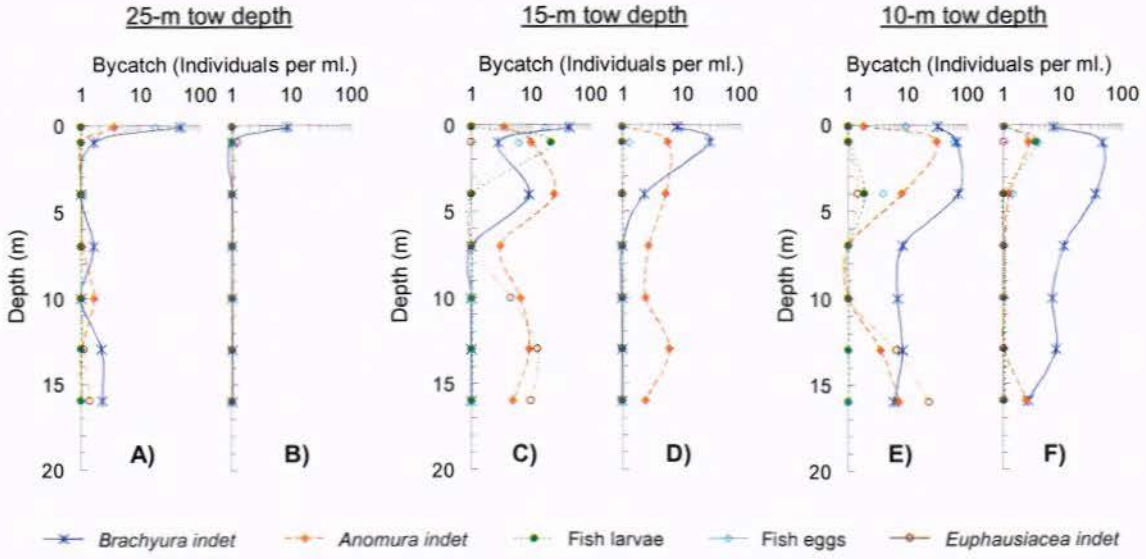

Fig. 12 Mean vertical bycatch profile before (A, C, E) and after (B, D, F) the bubble trawl for 25-m, 15-m and 10-m tow depth for 22 June 2008. See Table 3 for enhancement rates.

Table 3 Mean bycatch dehancement rates ($\varepsilon<1$) at different tow depths, June 2008.

Bycatch	25-m tow depth	15-m tow depth	10-m tow depth	ALL
Brachyura indet	77.6	26.9	40.8	48.4
Anomura indet	84.6	60.0	84.3	76.3
Fish larvae	70.3	96.4	12.0*	51.6
Fish eggs	98.2	93.7	91.9	94.6
Euphausiacea indet	22.2	95.2	95.3	70.9
Shrimp	75.5	52.7	62.2	63.5

* Enhancement

Bubble plume jellyfish flotation was observed to be effective particularly by the plume's largest bubbles, which reached the sea surface prior to surfacing of the main bubble plume; although upwelling from the main plume also lifted jellyfish. These observations were highly encouraging; however, quantification of bubble-plume jellyfish flotation was not done.

4 Discussion

4.1 Bubble upwelling and surface layer *Calanus* enhancement

The bubble trawl was highly successful at elevating *Calanus* concentrations in a thin surface layer. Surface enhancements, ε, as high as 1416% were observed in 2009 (Fig. 6). Although greater ε in surface layers were observed in 2008 in the presence of stratification, enhancement relative to the maximum in the water column, C_C, were far greater for the unstratified conditions of 2009 than 2008. In 2009, a *Calanus* trawl located at 20 m behind the bubble plume and at a depth of 1 m would have been increased the haul by 980% relative to elsewhere in the water column. These enhancements are dramatically larger than the effect of hull mixing, which moreover, could not lead to *Calanus* concentrations greater than elsewhere in the water column.

Bubble raft design also played a role. In 2008, the bubble raft created a bubble plume dominated by small bubbles, emphasizing attachment flotation. Further, these plumes were homogeneous at the sea surface, exhibiting convergence regions and presumably downwelling zones within the plume surfacing footprint. In 2009, the bubble raft was designed to create a strengthening, homogeneous bubble pulse, with the bubble sheet rise matching the bubble raft tilt leading to Q rapidly increasing with time. Visual observations suggest that large-scale, persistent near-surface eddies played an important role, by trapping bubbles (observed) and trapping *Calanus* (hypothesized). Certainly, the exponential *Calanus* profile in the upper few meters bears little resemblance to water-column characteristics or control *Calanus* profiles – double Gaussian. Fortuitously, stratification was negligible to at least 15 m (tow depth) for most of the 2009 study. For example, at 06:36 LT, salinity was constant to 20-m depth, over which temperature decreased only 0.1C. Stratification did increase towards the end of the study period for depths below 15 m; with temperature dropping from 4.9C at 15 m to 4.55C at 20 m, thus some entrainment of deeper water could have occurred and influenced flows. However, the bubble plume for the first meter or so above the bubble raft is in the acceleration phase, so the most significant fluid entrainment occurs somewhat shallower than the tow depth (the necking depth (Fanneløp and Webber, 2003)). Thus, entrainment flows at the bubble source likely were driven by a significantly smaller $<V_{up}>$ implying that deeper (denser) water entrainment was negligible.

Fluid motions originated by the towed bubble plume (Fig. 13) appeared to be more complex than for those originating from a stationary source, presumably due to the transient nature of towed bubble plume, the resultant bubble size segregation, and the interaction between persistent fluid motions and the rising bubbles (whose size distribution shifts towards smaller bubbles and thus lower total Q with time). Note, down-tow distance is equivalent to time; thus, Zone 1 becomes Zone 5 after a few minutes.

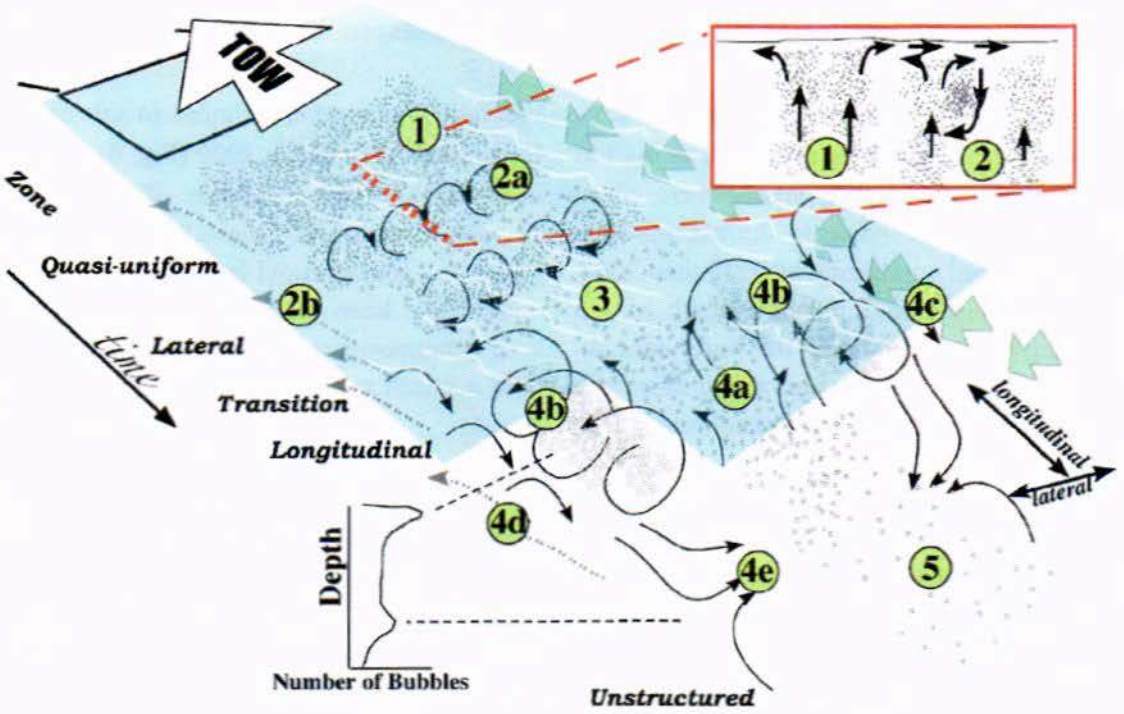

Fig. 14. Summary schematic of observed fluid motions and bubble spatial distribution for the transverse-element bubble raft. See text for description.

Where the bubble plume first surfaced (*Quasi-uniform Zone* (1)), bubbles showed no consistent spatial organization, rising in small and unsteady boils, as well as randomly in between. Bubbles here primarily were large; however, with increasing down-tow distance (time), bubble size generally decreased, as smaller, slower rising bubbles surface and the upwelling flow slows. Outwelling flows (horizontal surface intrusions spread in all directions, including in the tow direction. The bubble plume is surrounded laterally by a momentum plume (dashed arrows, *Zones* 2–4). Thus, by continuity, inwelling flows are likely at some depth, and were visible further down tow (*Zone* 4). In the *Lateral Zone* (2), bubbles were organized into alternating rotation linear vortices with bubbles trapped in their centre, separated by downwelling and upwelling zones. A proposed mechanism for the vortex formation is from the interaction between the outwelling flow when the upwelling flow is strongest, and the upwelling flow driven by bubbles later in the rising pulse (Fig. 14, inset). Needless to say, bubbles in the strongest upwelling flow surface first, thus with increasing down-tow distance (later in time), the upwelling and hence outwelling flow becomes weaker. As a result, the outwelling from the initial pulse in the downcurrent direction, is stronger then the up-tow direction outwelling, and over-rides it. This could lead to vortex formation from the transformation of vertical upwelling momentum into angular momentum. In fact, torroidal structures are seen for stationary point-source bubble plumes where fluid from the downwelling flow outside the upwards momentum flow is re-entrained in the main upwelling flow (Leckert and Imberger, 1993). Here, the tow geometry lends to linear rather than torroidal vortices.

Breakup of the lateral vortices, possibly due to instabilities is rapid, allowing trapped bubbles to escape in the *Transition Zone* (3). Shortly thereafter, two persistent (i.e., long), longitudinal vortices form in the *Longitudinal Zone* (4). The longitudinal vortices (4b) trap bubbles (rendering the vortices highly visible) for tens of seconds or longer, and surround a central upwelling (4a) region where small bubbles and fluid upwell. Outside the vortices are two longitudinally-oriented *Downwelling Zones* (4c), where bubbles are not observed rising, causing a sharp edge (tens of centimeters) to the location of the bubble plume. These downwelling zones are driven primarily by upwelled fluid, but also by weakly inwelling fluid, which is observed as sea surface foam concentration (and likely surfactants). The momentum plume (4d) is expected to broaden and weaken with time, and must surface outside the longitudinal vortices. There also likely is asymmetry in the momentum plume with respect to current; however, details of the momentum plume were not characterized in the field.

One hypothesis for the difference between the *Lateral* (2) and *Longitudinal* (4) *Zones* is that the bubble plume in the *Lateral Zone* (2) is of sufficient high density that the bubbles have "top hat distribution," leading to a relatively uniform upwelling flow over the area plume in a lateral sense. Meanwhile, the rapid evolution of upwelling flow as the largest bubbles arrive at the sea surface and then burst leads to more rapid changes in the upwelling flow in the longitudinal (time) direction than in the lateral direction. In contrast, in the Longitudinal Zone (4), bubbles primarily are small and at significantly lower concentration, thus the upwelling flow here likely is far weaker. In such case, momentum transfer at the plume edge could have shifted the velocity profile towards a Gaussian profile – i.e., strongest upwelling in the center. In such case, lateral outwelling is more easily driven than longitudial, because the upwelling flow strength decreases far more slowly longitudinally (time) than laterally (a hundredfold).

In the *Longitudinal Zone* (4), an inflow was observed at depth (4e), which drives bubbles towards the upwelling plume center, leading to a bimodal vertical bubble profile. Visibility was ~5 m, so this inflow is unassociated with plume processes at the tow depth. Near the surface, bubble densities are high because of vortex trapping, while a secondary higher density was observed at depth – likely there is downwelling – which leads to the aggregation. Finally, in the *Unstructured Zone* (5), small bubbles rise to the sea surface, leading to a clear "wake" effect, however, clear associated flow motions were not observed.

The tow direction was cross–current due to the need to avoid land, which could have played a role in the enhancement of surface *Calanus* concentrations. Specifically, currents would transport *Calanus* individuals across the bubble plume where they would interact with bubbles and turbulence associated with the bubble plume. Some of these drifting *Calanus* would become trapped in the upwelling flow due to bubble attachment, while others could find themselves trapped in eddies that are advected by the plume. Eddy trapping and steering is used in a bubble oil boom where entrained oil droplets were found to be very efficiently trapped and recirculated to the plume's up current side within the plume (McClimas et al., 2010). Currents also would transport *Calanus* upwelled by the momentum plume into the longitudinal eddies.

Because the enhancement, ε, for depths shallower than ~4 m was significantly above 1, but there was no significant dehancement, δ, (ε<1) for deeper depths, the increased *Calanus* in the water column must have been primarily from lateral bubble plume entrainment of *Calanus*. Some of the lateral entrainment enhancement could have arisen from deeper water (z>4 m), compensating in part the reduction in $C_T(z)$ due to vertical advection (upwelling) of a *Calanus* profile $C_C(z)$ that decreased with depth below 10-12 m. However, enhancements of 560–980% relative to the water column maximum are difficult to explain by deeper entrainment and upwelling as they would almost certainly have caused significant deviation from ε=1 for z>4 m. Given the absence of *Calanus* in the surface layer (C_C), lateral enhancement likely included an upwards component. Also, momentum plume upwelling, which surrounds the bubble plume, could have played a role through lateral *Calanus* entrainment.

4.2 Stratification and *Calanus* Bubble Trawl

Because a bubble plume does work lifting fluid against a density gradient, stratification is a dominant factor in *Calanus* bubble trawl performance. Although 2009 studies fortuitously were largely free of stratification in the upper 15 m (<0.15 g L^{-1} for upper 20 m) (Fig. 7A) conditions in 2008 were significantly stratified (Fig. 8A). Unsurprisingly, there was a strong relationship between stratification and *Calanus* enhancement (ε>1) and dehancement (ε<1).

At the sea surface, the rising upwelling flow becomes the outwelling flow. Where the rising fluid is denser (due to stratification), the outwelling flow has a sinking component. This sinking component depends on the density difference between the plume fluid and ambient, which is dependent on the stratification and the plume strength. Specifically, the buoyancy flux of a weak bubble plume is less able to support fluid against a density difference, leading to greater plume entrainment/detrainment, and as a result, a lower density difference between the outwelling fluid and the ambient. Here, plume scale can play a role, too. For example, lake stratification studies found that plume spreading for an area plume is less than for a point source–implying relatively lower entrainment/detrainment. McClimas et al. (2010) argued this is a scaling effect from the source elements, which are smaller than the area plume dimensions. As a result, an area plume should be more capable of lifting fluid against a stratification leading to a greater surface density difference. In extreme cases, the outwelling flow may form downdrafts – a condition to be avoided in a bubble trawl. In the 2008 study, the outwelling flow was weak, the upper ocean was highly stratified, and unsteady convergence zones (patches of bubble flotsam) were observed within the plume surfacing region (Zone 1).

By continuity, these convergence zones must be associated with downwelling flows, which would transport *Calanus* away from the surface layer. In general, plume induced downwelling has not been studied; however, it should be similar to single phase continuum flows in a downwards direction, albeit in the vicinity of the complex fluid motions associated with the bubble plume. The intrusion depth of the downwelled fluid should relate to stratification as well – mixing of the fluid during rise in the bubble plume means the equilibrium density is less than that of the water at its original entrainment depth (List, 1982). Thus, the exponential character of the *Calanus* profile after trawling (C_T - Fig. 6B) must arise from a combination of upwelling, outwelling, downwelling and intrusion

processes. Note, some of the shape of $C_T(z_T)$ could be a sampling artefact, because plume dimensions are broader, closer to the surface, so the shifting tow net position implies greater sampling time in the bubble plume for shallower depths. For an area plume, this broadening is a small factor, and the tow net generally was aligned with the bubble plume.

Investigation of the shift to positive enhancement (depth where *Calanus* detrainment + entrainment is positive) with respect to the density difference, ρ', found values of 0.3 to 0.6 g L^{-1}, suggesting a limit for this plume to lift water against stratification. For 25 and 10-m tows, ρ' was 0.4 and 0.3 g L^{-1}, respectively, suggesting tow depth was not a dominant factor. In contrast, the significantly lower stratification during the 15-m tow experiment, which supported a ρ' almost twice as large, suggests that a more appropriate scaling is dρ'/dz, as suggested by List (1982). Other factors, such as plume dimensions or, more specifically, whether the bubble source is an area or point likely is important too – an area source at sufficient depth acts like a point source. This depth effect was observed for the 25-m tow for the parallel-sparger bubble raft where the surfacing bubble plume exhibited boils rather than the largely heterogeneous surfacing flow created by the transverse-sparger bubble raft (from 15 m). Further, high air flow bubble plumes can transport water more readily against stratification, thus, Q likely plays a role in scaling. In these experiments, Q was the same for all bubble plumes (compressor maximum), except for dissolution reduction of Q for the 25-m tow. Clearly more than three data sets are needed to properly characterize the effect of stratification on area plumes.

Absent stratification, such as in the laboratory (McClimas et al., 2010), the strong lateral vortices observed in the field do not form. In the ocean, there always is some stratification which leads to a sinking tendency in the outwelling flow, wherein fluid re-entrainment into the upwelling flow creates a rotor. For the bubble trawl, weakening of the outwelling flow with time is proposed as driving this vortex (Fig. 13). Stratification also likely plays a role in the vortex strength and persistence. Specifically, a greater density difference ρ' could be expected to drive a stronger vortex, although the downwelling also transports fluid and *Calanus* away from the surface. Thus, there likely is an optimum density difference, with larger ρ' leading to most of the fluid being downwelled instead of supporting vortical motions. Stratification also likely affects negatively vortex persistence. Specifically, bubble size decreases with time as the larger bubbles surface first, leading to a decreasing Q and hence upwelling and outwelling flow. Because weaker flows are less effective at transporting fluid against stratification, stratification likely slowly "quenches" the outwelling flow.

4.3 Bubble plume generation

Two highly distinct approaches were used to generate bubble plumes during the two field test series, one used a flushed sparger, which tended to produce very small bubbles, and the second used a porous rubber hose that produced larger bubbles in the 1-2 mm size range. Size distributions were not measured in the field (i.e., at depth, tow, and pressurized) and significant deviations from laboratory results are likely.

A key advantage of the porous rubber hose sparger elements, aside from producing larger bubbles, is that resistance to air flow through the hose pores creates a significant internal overpressure relative to hydrostatic. As a result, small hydrostatic pressure changes from waves, and variations in tow depth and sparger element tilt, etc., have minimal effect on the bubble emission rate along the hose, yielding relatively uniform, steady state bubble emissions. In contrast, bubbles from a non-porous, drilled rubber tube were highly sensitive to hydrostatic pressure, such that portions of the hose under wave crests produced less to no bubbles. One disadvantage of the porous rubber hose arises from this pressure gradient across the tube wall; increasing flow rapidly increases the internal pressure towards regulator limitations. This limitation could be addressed by bundling multiple hoses together.

The flushed sparger approach clearly produced far smaller bubbles, which a video camera mounted on the raft imaged as milky in appearance. With regards to bubble processes, the smaller flushed sparger bubbles are less efficient at creating upwelling flows (Patro *et al.*, 2002), but more efficient at attachment (Jeuthe, H., University of Tromsø, Norway, pers. comm., 2008) than the larger bubbles from the porous rubber hose. Significantly, the observation that bubbles from the flushed sparger from 25-m depth did not always reach the surface strongly suggested that bubbles produced were dissolving during rise. Bubble dissolution reduces the buoyancy flux, reducing the plume's ability to transport fluid against stratification and maintain coherency against current and wave disruption.

To better understand the importance of bubble dissolution to bubble plume behavior, simulations were conducted with a numerical bubble propagation model (described in Rehder et al., 2009 and Leifer et al., 2006) for a range of bubble sizes and release depths in Arctic (i.e., cold) waters. Bubble dissolution occurs as a bubble rises due to the internal gases diffusing from the bubble with a rate determined by the concentration gradient across the interface (defined by Henry's Law equilibrium) and bubble size. Bubble dissolution occurs when bubble shrinkage from mass loss is faster than growth from decreasing hydrostatic pressure. Because nitrogen (oxygen is a relatively minor gas) is close to equilibrium in the ocean, hydrostatic pressure causes deeper bubbles to outgas more rapidly than shallower bubbles. As a result, with increasing initial depth, larger bubbles are needed to ensure that bubbles reach the sea surface.

Simulations for 6°C (Fig. 14) with a clean-dirty bubble transition at r~1300 μm (Patro et al., 2002) show that from 10 m with no upwelling flow–i.e., pure flotation, only bubbles with initial radius, r_o>~250 μm can reach the sea surface. In contrast, for 20 m, the bubble must be larger than r_o>~500 μm. The effect of temperature on V_B is important, for 20°C (most lab measurements), a r~100 μm bubble can make it to the sea surface from 10 m, while in Arctic waters r_o must be >~250 μm for the same conditions.

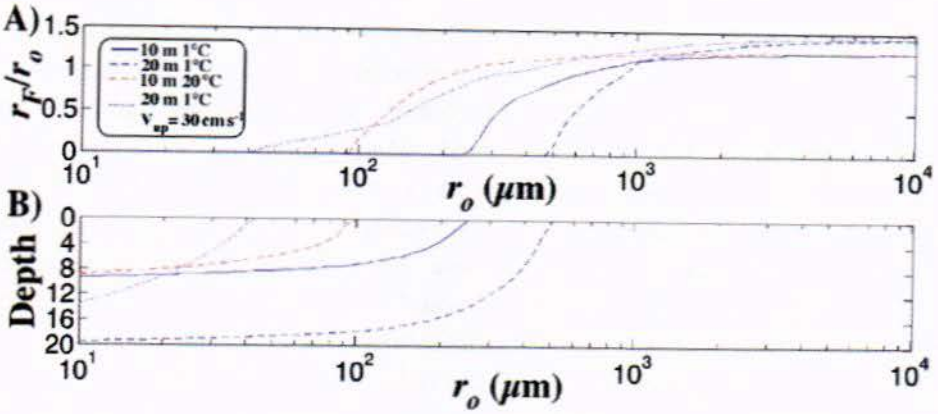

Fig. 15 Numerical simulation of air bubbles in Arctic water (1°C) for 10 and 20 m depth, for 10 m at 20°C, no upwelling, and for 1°C from 10 m with upwelling velocity, V_{up}, 30 cm s^{-1}. **A)** Ratio of final radius, r_F, to initial radius (r_o), **B)** Dissolution depth versus r_o. Data key on figure. See text for details.

Field operation of the flushed sparger also faced other challenges. For example, it required a very high water supply (1400 L min^{-1}) to adequately distribute the air-water mixture over the entire bubble raft, necessitating large water pumps on the towing vessel and a large working deck area for handling and storage of the large diameter water supply hose. The sparger element separation appeared to be too large, particularly at lower flow rates (upwelling study), where the plumes did not merge into a single plume. Specifically, the goal was to avoid having convergence zones and downwelling flows interior to the area bubble plume, as such flows represent a (potentially significant) loss of upwelling efficiency. However, lab tests show that bubble plumes with small bubbles are more susceptible to formation of boils (McClimas et al., 2010). Part of the underlying process likely is that the lower rise velocity of smaller bubbles leads them to be more easily trapped and advected in eddies, leading to a broader buoyancy spatial distribution. As a result, from 25 m, far stronger boils (relative to the outwelling velocities) were observed at the sea surface than for shallower depths for the longitudinal bubble raft. These boils represent a loss of coherence of plume-driven fluid motions, which should decrease fluid upwelling, V_{up} (increase entrainment/detrainment). Moreover, unlike a coherent bubble plume, which is surrounded by an upwelling momentum flow, bubble boils are surrounded by complex fluid motions including strong downward flows.

4.4 A continuous injection bubble pulse

The transverse-towed element bubble raft produced a truly novel bubble plume, continuously injecting bubbles into the same pulse. Where a bubble pulse is produced from a stationary area plume and Q increases as the bubble plume rises due to decreasing hydrostatic pressure, the increase is non-linear, and except for near the sea surface, small. For example, for a 20-m plume with V_{up}=20 cm s^{-1}, Q doubles after bubbles have risen for 50 s. In comparison, the towed bubble raft's Q for the first meter doubles after 1 second during which the plume has only risen ~0.5 m, with additional increases in Q from hydrostatic expansion. On the other hand, because the bubble plume is a pulse, fluid

acceleration is continuous. The upwelling flow generated was far less for the tow-parallel sparger bubble raft than for the tow-transverse sparger bubble raft due largely to the pulse-like nature of the bubble plume. Currently, bubble pulse behaviour, particularly for an area plume, remains completely uncharacterized, while this is the first reported continuous injection bubble pulse. Some aspects of a bubble plume with increasing bubble concentration could enhance a *Calanus* bubble trawl. For example, greater bubble concentration implies greater turbulence and more frequent bubble-*Calanus* interactions, making *Calanus* escape more difficult. Although an initial pulse of very high density could have been created, it would have had significantly greater turbulence, which likely would have led to more rapid conversion of the pulse into boils (coherent plume structures). Instead, we hypothesize that continuous injection along the path disrupts coherent plume structure development and provides more efficient upwelling.

4.5 Fluid motions and *Calanus* concentrations 2008

The rising bubble sheet was observed to fragment into linear bubble plumes with angular rotational motion that became boils at the sea surface. Persistent turbulence eddies were observed to trap bubbles and hypothesized to trap *Calanus*. Accordingly, laboratory observations of *Calanus* entrained in single bubble turbulence wakes, suggest they face difficulty jumping effectively in the highly turbulent environment associated with bubbles (Jeuthe, H., University of Tromsø, Norway, pers. comm., 2008). Therefore, we propose that vortex trapping is enhanced by jump confusion, leading to enhanced *Calanus* concentration. When bubbles escape the vortices, both through random chance (greater for larger bubbles) and as the vortices slow down, they create small scale, local upwelling that also will transport *Calanus* towards the sea surface.

4.6 Synergistic upwelling and flotation

Although the focus of the transverse-sparger bubble raft was attachment flotation and that of the parallel-sparger bubble raft was upwelling flotation, both processes occurred for both rafts. Moreover, the two processes are synergistic, *Calanus* with attached bubbles likely have greater difficulty escaping from the bubble plume, including when trapped in a turbulence vortex, and the added buoyancy increases their upwards velocity. Further, for *Calanus* to escape the bubble trawl, they need to jump away from the bubbles, which likely is less efficient for individuals with attached bubbles.

One interesting and potentially important feature of vortex trapping is that it places zooplankton and bubbles in close proximity with numerous opportunities for bubble-zooplankton interaction and aggregation formation. Thus, upwelled zooplankton likely become trapped in vortices, while the upwelling flow prevents downward escape and lateral escape for zooplankton even at the plume edge likely is inefficient because the inflow and because the jump response is random when confronted by bubbles (Jeuthe, 2009). Further, some fraction of *Calanus* that do escape may be re-entrained in the upwelling flow in the bubble plume. Thus, significant *Calanus* could have some bubble attachment, aiding the upwelling process.

4.7 Bubble trawl bycatch reduction

The upwelling flow and the vortices appeared to be effective at trapping other copepod sized species, although healthy fingerlings were able to escape the upwelling and largely immune to attachment. The towed bubble plume reduced 65% of all types of bycatch organisms, which were in the path of the bubble plume. The greatest reduction was for crabs (in different larvae stadiums) and fish eggs, which initially were concentrated in a shallow layer (<3 m) and likely were floated towards the sea surface by the bubble plume. At the surface, the effect of the outwelling flow apparently removed them laterally, making them unavailable for the sampling nets. Because sampling was not performed at the bubble plume edges, the fate of these bycatch organisms is unclear. The bubble plume's effect upon fish larvae and especially upon small fish seems different from that for crabs larvae and fish eggs. Accordingly, while bubble attachment process may have enhanced the flotation of crabs and fish eggs (presumably because of hair and stickiness of fish eggs); bubble attachment to fish larvae and fingerlings it seems highly improbable. Also, visual evidence of small fish swimming inside the bubble plume suggests that fish larvae and fingerlings may have actively avoided the bubble plumes.

The largest (~3-4 mm diameter) bubbles surfaced first and apparently were highly effective for jellyfish flotation. This not only represents a great advantage for bubble-enhanced *Calanus* harvesting, but also for conventional fine-meshed trawls for *Calanus* and other fisheries. For example, jellyfish flotation could divert jellyfish from the path of the trawl, avoiding associated problems with net clogging, catch damage, sorting, etc. Jellyfish flotation appears distinct from *Calanus* flotation, in that due to the morphology of the jellyfish, bubbles readily are trapped in their body, leading to more effective buoyant rise. For example, jellyfish were very common in 2008 and were observed floating at the sea surface with entrapped bubbles. Although the bubble trawls were not designed to effectively divert jellyfish through flotation; such diverters could be very useful for improving the *Calanus* fishery.

4.8 Future Study Needs

The current study highlighted that bubble plume fluid motions responsible for enhancing the *Calanus* into a surface layer were more complex than for a simple upwelling flow, involving lateral entrainment. Future efforts should quantify *Calanus* profiles in three dimensions (time, depth, and transverse). Although spatial resolution was improved in 2009 through more plankton tow nets, the surface layer was poorly resolved, while deeper plankton nets would have aided interpretation. The data suggest significant lateral entrainment from shallow and near shallow waters, which could be investigated by varying the tow depth. Finally, vortex bubble trapping supported the vortex *Calanus* trapping hypothesis as a key process underlying the significant shallow *Calanus* enhancement. This hypothesis needs validation by video or other sampling methods. Video image analysis also could test the role of bubble attachment in synergistically improving bubble trawl performance.

Study results highlighted the critical role of stratification in bubble-plume processes related to *Calanus* bubble trawl performance. Thus, more frequent or preferably continuous CTD profile data would have improved significantly data interpretation, removing a large source of uncertainty. For example, the arrival time of the shallower stratified fluid layer towards the end of 30 April 2009 was unknown. For the stratified field data, analysis suggested continuous loss of deeper upwelled *Calanus* to the water column, rather than into a surface layer. The associated fluid motions, which may be driving these processes, need better characterization. One approach would be to use continuous, controlled dye injection with fluorometric profiling to map detrainment quantitatively. Similarly, fluorometry could determine the fraction of time plankton nets are in the bubble plume–in these field tests, the plankton tow nets periodically drifted out of the bubble plume. Thus, reported enhancements are conservative.

Finally, significant deployment challenges were encountered, thus future efforts to improve bubble raft robustness are needed.

4.9 Conclusions

The area bubble plume-enhanced *Calanus* harvesting technology, presented in this paper, is a unique and novel design that improved copepod catch rates, reduced bycatch, and significantly decreased energy consumption during towing by allowing for a smaller collector. Results showed very strong *Calanus* enhancement relative to elsewhere in the water column in a thin surface layer during tests in the absence of stratification. Stratification was a dominant factor affecting bubble trawl performance; however, data were insufficient to characterize stratification's effect on bubble plume fluid motions beyond fluid-ambient density difference.

Investigation of bubble generation approach suggested small bubbles are problematic, particularly for deeper tow depths where dissolution becomes significant, compared to larger bubbles. Large bubble generation was effective by pressurizing a porous rubber hose – the pressure difference across the hose walls prevented hydrostatic pressure changes (swell) from causing emission variability along the sparger elements, in contrast to a drilled rubber hose. The current bubble trawl design, while appropriate for these field tests, lacked robustness for commercial application.

Although highly promising, study results highlighted significant areas of critical need for further study. More sophisticated measurement approaches are needed to improve data collection, such as using fluorometric profiling in conjunction with continuous metered dye injection, continuous CTD profiling, and a larger dataset for a field trial. Bycatch results were highly promising; however, further study is needed to characterize bubble trawl advantages, including jellyfish diversion.

Acknowledgments

We thank Thomas McClimans from SINTEF Fisheries and Aquaculture AS, Sünnje Basedow and Manu Sistiaga from the University of Tromsø for revising and commenting the manuscript; Jon Terje Eilertsen for help with the instruments on board Jan Mayen; and Snorre Angell, Ivan Tatone, Trond Larsen and Lasse Rindahl for their valuable assistance on field work. Thank the crews of the Hyas and Jan Mayen. This work was funded by the Research Council of Norway through the Oceans and Coastal Areas Program (MAROFF), project 178421/S40, "Harvesting zooplankton by bubble flotation".

5 References

Aksnes D.L. and Blindheim J. (1996) Circulation patterns in the North Atlantic and possible impact on population dynamics of *Calanus finmarchicus. Ophelia* **44:**7–28.

Aseda, T., Imberger, J., 1993. Structure of bubbles plumes in linearly stratified environments. *J. Fluid Mech.* 249: 35-57.

Dahle, T., Kaartvedt, S., 2000. Diel patterns in stage-specific vertical migration of *Calanus finmarchicus* in habitats with midnight sun. ICES J. Mar. Sci. 57, 1800-1818.

Falkenhaug, T., Timonin, T., Tande, K., 1997. Abundance and distribution of numerical important species of zooplankton in summer and winter periods of 1990 and 1991 in North Norwegian fjords. *J. Plankton Res.* 19(4), 449-468.

Fanneløp, T.K., Sjøen, K., 1980. Hydrodynamics of underwater blowouts. In: Proc. AIAA 18th Aerospace Sci. Meeting, Passadena, CA.

Fanneløp, T. K., Hirschberg, S., Küffer, J., 1991. Surface current and recirculating cells generated by bubble curtains and jets, *Journal of Fluid Mechanics* Digital Archive, 229(-1), 629-657.

Fanneløp, T. K., Webber, D. M., 2003. On buoyant plumes rising from area sources in a calm environment, *Journal of Fluid Mechanics*, 497(-1), 319-334.

Grace, J., Sowyrda, A., 1970. The development and evaluation of a pneumatic barrier for restraining surface oils in a river. *Journal of Water Pollution Control Federation*, 42(12), 2074-2093.

Johnson, B. D., Cooke, R. C., 1980. Organic Particle and Aggregate Formation Resulting from the Dissolution of Bubbles in Seawater. *Limnology and Oceanography*, 25(4), 653-661.

Kattner, G. and Krause, M., 1987. Changes in lipids during the development of *Calanus finmarchicus* s.l. from Copepodid I to adult. *Mar. Biol.*, **96**, 511–518.

Lalli, C. M., Parsons, T. R., 1997. *Biological Oceanography*. The Open University.

Leifer, I., Boles, J., 2005. Measurement of marine hydrocarbon seep flow through fractured rock and unconsolidated sediment. *Marine and Petroleum Geology*, 22(4), 551-568.

Leifer, I., Jeuthe, H., Gjøsund, S.H., Johansen, V., 2009. Engineered and natural marine seep, bubble driven buoyancy flows. *J. Phys. Oceanography*, 39(12), 3071-3090.

Leifer, I., Clark, J.F., Chen, R.F., 2000a. Modifications to the local environment by natural marine hydrocarbon seeps. *Geophys. Res. Let.*, 27, 3711-3714.

Leifer, I., Luyendyk, B., Boles, J., Clark, J.F., 2006. Natural marine seepage blowout: Contribution to atmospheric methane. *Global Biogeochemical Cycles*, 20, doi:10.1029/2005GB002668.

Leifer, I., Patro, R. K., 2002. The bubble mechanism for methane transport from the shallow sea bed to the surface: A review and sensitivity study. *Continental Shelf Research*, 22(16), 2409-2428.

Leifer, I., Patro, R. K., Bowyer, P., 2000b. A study on the temperature variation of rise velocity for large clean bubbles. *Journal of Atmospheric and Oceanic Technology*, 17(10), 1392-1402.

Leifer, I., Judd, A., 2002. Oceanic methane layers: A bubble deposition mechanism from marinehydrocarbon seepage. *Terra Nova* **16**:471-485.

Lemckert, C.J., Imberger, J., 1993. Energetic bubble plumes in arbitrary stratification. *J. Hydraul. Eng.* 119: 680-703.

List, E.J., 1982. Turbulent jets and plumes. *Ann. Rev. Fluid Mech.* 14, 189–212.

Mao, L., Yoon, R.-H., 1997. Prediction flotation rates using a rate equation derived from first principles. *Intnl. J. Miner. Proc.*, 51: 171-181.

McClimas, T., Leifer, I., Gjøsund, S., Grimaldo, E., Daling, P., Leirvik, F., 2010. On pneumatic oil barriers: The promise of bubble rafts. Oceanic Eng, IN PREPARATION

Mari, X., 1999. Carbon content and C:N ratio of transparent exopolymeric particles (TEP) produced by bubble exudates of diatoms. *Mar. Ecol. Prog. Ser.* 183: 59-71.

McDougall, T.J., 1978. Bubble plumes in stratified environments. *J. Fluid Mech.* 85, 655-672.

McGinnis, D. F., Lorke, A., Wüest, A., Stöckli, A., Little, J. C., 2004. Interaction between a bubble plume and the near field in a stratified lake, Water Resour. Res., 40.

Milgram, J.H., 1983. Mean flow in round bubble plumes. J. Fluid Mech. 133, 345-376.

Mizukawaa, K., Takada, H., Takeuchi, I., Ikemoto, T., Omori, K., Tsuchiya, K., 2009. Bioconcentration and biomagnification of polybrominated diphenyl ethers (PBDEs) through lower-trophic-level coastal marine food web, Marine Pollution Bulletin, *58*(8), 1217-1224

Nicol, S., Endo, Y., 1999. Krill fisheries: Development, management and ecosystem implications. Aquat. Living Resour., 12(2), 105-120.

Patro, R.K., Leifer, I., Bowyer, P., 2002. Better bubble process modelling: Improved bubble hydrodynamics parameterization. In: *Gas Transfer at Water Surfaces*, edited by M.Donelan, et al., pp. 315-320, American Geophysical Union, Washington.

Persechini, M.A.M., Jota, F.G., Peres, A.E.C., 2000. Dynamic model of a flotation column. Minerals Engineering, 13: 1465-1481.

Rehder, G.; Leifer, I.; Brewer, P.G.; Friederich, G.; Peltzer, E.T., 2009. Controls on methane bubble dissolution inside and outside the hydrate stability field from open ocean field experiments and numerical modeling. Mar. Chem., 114(1-2): 19-30.

Rensen, J., Roig, V., 2001. Experimental study of the unsteady structure of a confined bubble plume. Int. J. Multiphase Flow, 27: 1431-1449.

Ries, I. R. and Fanneløp, T. K., 1998. Recirculating flow generated by line-source bubble plumes. Journal of Hydraulic Engineering, 124, 932-940.

Sato, K. and Sato, T., 2001. A study on bubble plume behavior in stratified water. J Mar Sci Technol., 6: 59–69.

Simiano, M., Zboray, R., De Cachard, F., Lekehal, D., Yadigaroglu, G., 2006. Comprehensive experimental investigation of hydrodynamics of large-scale, 3D, oscillating bubble plumes. Int. J. Multiphase Flow, 32: 1160-1181.

Singleton, V. L., Gantzer, P., Little, J.C., 2007. Linear bubble plume model for hypolimnetic oxygenation: Full-scale validation and sensitivity analysis. Water Resour. Res., 43.

Schadlow, G., 1992. Bubble plume dynamics in a stratified medium and the implications for water quality amelioration in lakes. Water Resource Research 28(2): 313-321.

Solomon, E.A., Kastner, M., MacDonald, I.R., Leifer, I., 2009. Considerable methane fluxes to the atmosphere from hydrocarbon seeps in the Gulf of Mexico. Nature Geoscience, 2: 561-565.

Skjoldal, H.R.E., 2005. *The Norwegian Sea Ecosystem*, Tapir Academic Press.

Tande, K. S., Miller, C.B., 2000. Population dynamics of *Calanus* in the North Atlantic: Results from the trans-Atlantic study of *Calanus finmarchicus*. ICES J. Mar. Sci. 57(6), 1527-1527.

Topham, D.R., 1975. Hydrodynamics of an oil well blowout. Beaufort Sea Tech. Rep., Ocean Sci., Sidney BC, No 33.

Unstad, K., Tande, K., 1991. Depth distribution of *Calanus finmarchicus* and *C. glacialis* in relation to environmental conditions in the Barents Sea. Polar Research, 10(2), 409-420.

Wu, J., 1995. Mechanisms of animal cell damage associated with gas bubbles and cell protection by medium additives. J. Biotech. 43: 81-94.

Wüest, A., Brooks, N.H., Imboden, D.M., 1992. Bubble plume modeling for lake restoration, Water Resource Research, 28(12), 3235-3250.

Nomenclature

Q	(L min^{-1})	Air flow (corrected to STP)
Q_A	(L min^{-1})	Air flow per square meter (corrected to STP)
Q^b	(L min^{-1})	Power Law
r	(μm)	Bubble spherical radius
t	(sec)	Transit time
V	(cm s^{-1})	Velocity
V_{up}	(cm s^{-1})	Vertically-averaged plume upwelling velocities
V_{AG}	(cm s^{-1})	Bubble-copepod aggregate velocity
T	(C°)	Temperature
S	(ppm)	Salinity
ρ	(mg L^{-1})	Density
F	(mg L^{-1})	Fluorescence
z	(m)	Depth
z_0	(m)	Dye release depth
z_T	(cm)	Depth of sampling net mouth centre
C_C	(ml)	Catch of control nets 1
C_{C2}	(ml)	Catch of control nets 2
C_{Cm}	(ml)	Mean catch of C_{C1} and C_{C2}
C_T	(ml)	Catch of test nets 1
ε		ε > 1 Enhancement, ε < 1 Dehancement. Defined as C_T/C_C.